Elsevier Editorial System(tm) for Advances in Space Research
Manuscript Draft

Manuscript Number: ASR-D-11-00425

Title: Adaptation of a single-channel generalized method for the estimation of water surface temperature by means of Landsat 7 ETM+ thermal infrared data. Case study: Embalse del Río Tercero (Córdoba, Argentina).

Article Type: ES

Keywords: water surface temperature; reservoir; cooling system; nuclear power plant; single-channel generalized method; atmospheric water vapor.

Corresponding Author: Mss Anabel Lamaro, Ph. D. Student

Corresponding Author's Institution: Facultad de Ciencias Naturales y Museo, Universidad Nacional de La Plata

First Author: Anabel Lamaro, Ph. D. Student

Order of Authors: Anabel Lamaro, Ph. D. Student; Alejandro Mariñelarena, Ph. D.; Sandra E Torrusio, Ph. D.; Silvia E Sala, Ph. D.

Abstract: Monitoring of warm distribution in water is fundamental to understand the performance and functioning of reservoirs and lakes. Surface water temperature is a key parameter in the physics of aquatic systems processes since it is closely related to the energy fluxes through the water-atmosphere interface. Remote sensing applied to water quality studies in inland waterbodies is a powerful tool that can provide additional information impossible to achieve by other means. The combination of good real-time coverage, spatial resolution and free availability of data makes Landsat system a good choice. Many papers have developed algorithms to retrieve surface temperature (principally, land surface temperature) from at-sensor and surface emissivity data. The aim of this study is to adapt the single-channel generalized method developed by Jiménez-Muñoz and Sobrino (2003) for the estimation of water surface temperature by Landsat 7 ETM+ thermal bands. We choose Embalse del Río Tercero (Córdoba, Argentina) as case study because is a reservoir affected by the outlet of the cooling system of a nuclear power plant, which thermal plume could influence the biota's distribution and biodiversity. These characteristics and long term studies make it a very interesting place to test the methodology.
In the method presented here (AWVM), we consider a constant water emissivity value (0.9885) and we compare the results with radiative transfer classic method (RTM). Values of estimated and observed water surface temperatures obtained by the two compared methods were correlated applying a simple regression model. Correlation coefficients were significant (R2: 0.9426 for AWVM method and R2: 0.9584 for RTM method) while their standard errors were acceptable in both cases. Nevertheless, AWVM could estimate rather small differences in temperature between sites consistently with the results obtained in field measurements, besides it has the advantage that it only uses values of atmospheric water vapor and it can be applied to different thermal sensors using the same equation and coefficients.

Suggested Reviewers: Antonio Gagliardini Dr.
Centro Nacional Patagónico - CONICET

agaglia@cenpat.edu.ar

Carlos Bonetto Dr.
Instituto de Limnología "Dr. Raúl A. Ringuelet". CONICET
bonetto@ilpla.edu.ar

Juan Carlos Jiménez Muñóz Dr.
Global Change Unit, Department of Thermodynamics, Faculty of Physics, University of Valencia
jcjm@uv.es

Raúl Rivas Dr.
Universidad del Centro
rrivas@rec.unicen.edu.ar

Adaptation of a single-channel generalized method for the estimation of water surface temperature by means of Landsat 7 ETM+ thermal infrared data. Case study: Embalse del Río Tercero (Córdoba, Argentina).

A. A. Lamaro [a], A. Mariñelarena [b,c], S. E. Torrusio[d, e] , S. E. Sala[a]

[a.] *Departamento Científico Ficología, Facultad de Ciencias Naturales y Museo, Universidad Nacional de la Plata, Paseo del Bosque s/n (1900), La Plata, Argentina. E-mail: analamaro@fcnym.unlp.edu.ar . Telephone: 54-221-425-7744. Fax. 54221-4257527*
[b.] *Comisión Investigaciones Científicas, Provincia de Buenos Aires, Argentina.*
[c.] *Instituto de Limnología "R. Ringuelet", Universidad Nacional de la Plata, CONICET, Argentina.*
[d.] *Facultad de Ciencias Naturales y Museo, Universidad Nacional de la Plata, Argentina*
[e.] *Comisión Nacional de Actividades Espaciales, Argentina.*

Abstract

Monitoring of warm distribution in water is fundamental to understand the performance and functioning of reservoirs and lakes. Surface water temperature is a key parameter in the physics of aquatic systems processes since it is closely related to the energy fluxes through the water-atmosphere interface. Remote sensing applied to water quality studies in inland waterbodies is a powerful tool that can provide additional information impossible to achieve by other means. The combination of good real-time coverage, spatial resolution and free availability of data makes Landsat system a good choice. Many papers have developed algorithms to retrieve surface temperature (principally, land surface temperature) from at-sensor and surface emissivity data. The aim of this study is to adapt the single-channel generalized method developed by Jiménez-Muñoz and Sobrino (2003) for the estimation of water surface temperature by Landsat 7 ETM+ thermal bands. We choose Embalse del Río Tercero (Córdoba, Argentina) as case study because is a reservoir affected by the outlet of the cooling system of a nuclear power plant, which thermal plume could influence the biota's distribution and biodiversity. These characteristics and long term studies make it a very interesting place to test the methodology.

In the method presented here (AWVM), we consider a constant water emissivity value (0.9885) and we compare the results with radiative transfer classic method (RTM). Values of estimated and observed water surface temperatures obtained by the two compared methods were correlated applying a simple regression model. Correlation coefficients were significant (R^2: 0.9426 for AWVM method and R^2: 0.9584 for RTM method) while their standard errors were acceptable in both

cases. Nevertheless, AWVM could estimate rather small differences in temperature between sites consistently with the results obtained in field measurements, besides it has the advantage that it only uses values of atmospheric water vapor and it can be applied to different thermal sensors using the same equation and coefficients.

Keywords: water surface temperature; reservoir; cooling system; nuclear power plant; single-channel generalized method; atmospheric water vapor.

1. Introduction

Reservoirs are built for different purposes like drinking water supply, flood control, irrigation, or power generation (Casamitjana et al., 2003). Water temperature governs most of the chemical and biochemical processes in aquatic ecosystems. Monitoring of warm distribution in water is fundamental to understand the performance and functioning of reservoirs and lakes (Kimmel et al., 1990) and, its survey is important for water quality management, land-use, and hydrological studies (Kay *et al.*, 2005). Surface water temperature is a key parameter in the physics of aquatic systems processes since it is closely related to the energy fluxes through the water-atmosphere interface.

Water temperature surveys using conventional limnological sampling are expensive and time-consuming. Remote sensing applied to water quality studies in inland waterbodies is a powerful tool that can provide systematic and periodic coverage and also additional information from the non-visible regions of the spectrum impossible to achieve by other means (Dash et al., 2002; Novo et al., 2006; Alcântara et al., 2009). Moreover, satellite information allows obtaining data in digital format that can be easily combined with other geographic information and used to generate quantitative models (Chuvieco, 2002) and makes possible the reduction of field sampling frequency and costs. The success of water quality parameters quantification in inland environments depends on water characteristics and the sensor used. The combination of good real-time coverage, spatial resolution and free availability of data makes Landsat system a good choice for studying this kind of waterbodies.

During late 20th century, rapid technological advances resulted in increased availability of thermal infrared images and methodologies to calibrate and interpret them. Studies were performed using these data for mapping water surface temperature, especially in places with marked variations

-e.g. cooling channels of nuclear power plants, hot springs, etc.- (Gibbons and Wukelic, 1989, Mustard et al. 1999, Cherkauer et al. 2005, Zoran et al., 2005, Ahn et al. 2006, Alcântara et al., 2010).

All the energy exchanges between water mass and atmosphere take place within the very thin surface skin layer that can be remotely sensed. Temperature in this layer is typically cooler than the bulk water temperature so a critical factor to consider is the relationship between these temperatures. Evaporative cooling, wind speed and diurnal energy fluxes affect this complex relationship, nevertheless Yokoyama et al. (1995) and Schneider and Mauser (1996) demonstrated that remotely measured skin temperatures are representative of bulk water temperatures.

Emitted thermal infrared radiation (TIR, λ = 8 to 14 µm) can be used to measure temperature of the water surface layer of approximately 100 µm (Kishino et al., 2000, Donlon et al., 2002, Kumar et al., 2003; Kay et al., 2005, Becker & Daw, 2005). After removal of atmospheric and emissivity effects, recovered temperatures should be similar for all TIR sensor bands. Temperature differences between bands can also be consequence of sensor calibration problems, instrument noise, and in-scene spectral variability from nonwater materials (Kay et al., 2005).

Many papers have developed algorithms to retrieve surface temperature (principally, land surface temperature) from at-sensor and surface emissivity data. In the case of Landsat platform, with one thermal band, the only method that can be applied is a single channel one. Traditionally, the main disadvantages of this kind of method are that some atmospheric parameters are needed for the estimation and in addition, they cannot be used for other thermal sensor (Jiménez-Muñoz and Sobrino, 2003).

Jiménez-Muñoz and Sobrino (op. cit.) have developed a generalized single-channel method for retrieving land surface temperature from remote sensing data, called here as: *atmospheric water vapour method (AWVM)*. This algorithm, assuming that emissivity is known, only uses the total atmospheric water vapor content, the effective wavelength of the sensor and the at-sensor data (brightness temperature or at-sensor radiance). Land surface emissivity must be estimated, and different methods can be applied (Becker and Li, 1995; Goïta and Royer, 1997; Sobrino and Raissouni, 2000, Gillespie et al., 1998) while, in water surfaces, emissivity can be considered constant. In this paper we followed Snyder et al. (1998) who classified fourteen “emissivity classes” and presented their emissivity models and values for each emissivity class by combining various spectral component measurements with structural factors, based on MODIS thermal channels 31 and 32.

The aim of this study is to adapt the single-channel generalized method *(*Jiménez-Muñoz and Sobrino, 2003) for the estimation of water surface temperature by Landsat 7 ETM+ thermal bands. Embalse del Río Tercero is a reservoir affected by the outlet of the cooling system of a nuclear power plant, which thermal plume could influence the biota's distribution and biodiversity (Mariazzi et al., 1981, 1989). These characteristics and long term studies make it a very interesting place to test the methodology.

2. Materials and methods

2.1. Study area

Embalse del Río Tercero (ERT) (32º 11'S, 64º 25'W) is a medium size reservoir (5400 Hm^3, 46 Km^2, 45 m max. depth, 12 m mean depth, 0.44 y mean residence time), located in the center of Argentina, in the province of Córdoba (Fig. 1). The reservoir was built in 1936 for flood control, irrigation and hydroelectric purposes. Since 1983 water level fluctuations are regulated by requirement of a nuclear power plant of 600 MW, which uses its water for cooling purposes. The water inflow to the nuclear plant is located at 15 m deep in the Garganta area (G). Water temperature raiseS up 7º C in the cooling system and the outflow is directed through an open cooling channel of 6 km to the southern sector of the reservoir and discharges in a tributary, the Quillinzo River (Mariazzi et al., 1992).

As part of a monitoring program, since 1996 several physical, chemical and biological properties of the ERT waters are surveyed bimonthly (Mariñelarena et al., annual reports). Surface water temperature is measured at stations PAA, PC, M1, M2, C, G and D. Results have shown that warmer water released at Quillinzo River forms a thermal plume most of the time restricted to the river channel.

According to these reports, temperature in station G is always lower than that of stations PM1 and PM2. The differences between stations PM1 and G are 3 to 8 ºC (average 4.3 ºC, n = 74), while between stations PM2 and G differences are 0.5 to 5 °C (average 2.4 ºC, n=74) Mariñelarena (pers. comm.). Nevertheless, in a few dates in 15 years, the temperature of PM2 was lower than that of station G, due to programmed nuclear plant shutdowns and the effect of low temperature of Quillinzo River waters.

2.2. Remote sensing and water surface temperature estimation

In this work we used images from Landsat 7 ETM$^+$ (Path/Row: 229/82). This sensor has a unique thermal band (band 6) divided in two: low gain band (B6L) and high gain band (B6H), with a spectral resolution from 10.4 to 12.5 µm and a spatial resolution of 60 m covering a surface of 3.600 m^2 per pixel (0.36 ha). Images were obtained from the website of the United States Geological Survey (USGS) (http://glovis.usgs.gov/). They were in the UTM projection system, with WGS84 as ellipsoid and datum. They were resampled to 30 m of spatial resolution.

The criteria for the selection of images were:

(1) Existing *in situ* data in ± 3 days to the satellite passes.
(2) Images from different seasons in order to find temperature differences.
(3) 0% cloud cover when possible.
(4) No heavy rainfall prior to the image to minimize the effects of changes in water surfaces that disturb the estimates.

Selected images were: March 19th, 2000, August 13rd, 2001, August 16th, 2002 and July 10th, 2006 and November 15th, 2006.

Software ENVI 4.3 (Research Systems, Inc) was used for digital processing of images and application of algorithm.

2.2.1. Generation of "water images"

Definition of the specific shoreline for each image is critical to eliminate areas that are not representative of open waters and give inaccurate values of temperatures near the coast (Wang et al., 2008). In order to select pure water pixels, an unsupervised classification of near-infrared band (Band 4) was made. These classes were used as a mask for obtaining the desired image, thus eliminating the areas of land.

2.2.2. Radiometric conversion

Conversion of digital numbers (DN) to physical variables (radiance, reflectance and temperature) is very useful in the interpretation of images and to compare data from the same sensor over time or between sensors (Chuvieco, 2002). Digital processing for this conversion involves two main steps: radiometric calibration (Wukelic *et al.*, 1989) and atmospheric correction (Cooper and Asrar 1989).

DN values were converted to at-sensor radiance by applying the gain and bias of the detectors (Irish, 2006):

$$L_\lambda = \text{gain} * \text{DN} + \text{bias} \quad (1)$$

Where:

$L\lambda$ = uncorrected spectral radiance at λ wavelenght in W*m^2*sr*µm.

DN = digital number

gain and bias = calibration parameters of detectors (See Table 1).

2.2.3. Calculation of at-sensor radiative temperature (Tsat)

Radiance values calculated in Eq. (1) were converted to at-sensor radiative temperature using the following equation based on Planck's law (Wukelic et al., 1989):

$$T_{sat} = \frac{K_2}{\left[\ln\left(\frac{K_1}{L_\lambda} + 1\right)\right]} \quad (2)$$

Where:

$\mathbf{T_{sat}}$ =at-sensor radiative temperature (K)

K_2 and K_1= ETM+ thermal constants. K_2= 666.09 W*m^2*sr*µm and K_1 =1282.71 º K (Chander et al., 2009).

L_λ= uncorrected spectral radiance at λ wavelength in W*m^2*sr*µm.

2.3. Methods for water surface temperature estimation

2.3.1. Atmospheric water vapor method (AWVM) (adapted from Jiménez-Muñoz and Sobrino, 2003)

Water emissivity value was considered to be 0.9885 according to Sydner et al. (1998). Surface temperature calculation (Ts), the equation applied is as follows:

$$T_s = \gamma\left[\varepsilon^{-1}\left(\psi_1 L_\lambda + \psi_2\right) + \psi_3\right] + \delta \quad (3)$$

Where:

γ = see below, Eq. (7).

ε = water emissivity

L_λ= uncorrected spectral radiance calculated in Eq. (1).

ψ_1, ψ_2 y ψ_3= atmospheric functions were calculated by a simulation procedure with MODTRAN 3.5 (Jiménez-Muñoz and Sobrino, 2003).

From these values it is easy to obtain the atmospheric functions for every wavelength and for every atmospheric water vapor content (Jiménez-Muñoz and Sobrino, 2003). The values of these functions were calculated by:

$$\psi_1 = 0.14714\, w^2 - 0.15583\, w + 1.12340 \quad (4)$$

$$\psi_2 = -1.1836\, w^2 - 0.37607\, w - 0.52894 \quad (5)$$

$$\psi_3 = -0.04554\, w^2 + 1.8719\, w - 0.39071 \quad (6)$$

Where:

w = atmospheric water content obtained from http://weather.uwyo.edu/upperair/sounding.html, including date, hour and geographic location.

δ= see below, Eq. (8)

γ was calculated from:

$$\gamma = \left\{\frac{C_2 L_\lambda}{T_{sat}^2}\left[\frac{\lambda_{ef}^4}{C_1} L_\lambda + \lambda_{ef}^{-1}\right]\right\}^{-1} \quad L_{\lambda = \text{gain} * \text{DN} + \text{bias}} \quad \gamma \quad (7)$$

Where:

C_2= 14387.7 µm*K

C_1 = 1.19104*10^8 W µm^4

λ_{ef} = effective wavelength (11.45 µm)

L_λ = uncorrected spectral radiance calculated in Eq. (1).

T_{sat} = at-sensor radiative temperature (K) calculated in Eq. (2).

δ was calculated from:

$$\delta = -\gamma L_\lambda + T_{sat} \quad (8)$$

Where:

L_λ: uncorrected spectral radiance calculated in Eq. (1).

$\mathbf{T_{sat}}$: at-sensor radiative temperature (K) calculated in Eq. (2).

2.3.2. Radiative Transfer Method (RTM)

The atmospheric correction of the radiance of thermal band involves the removal of atmospheric effects that contribute to the signal received by the sensors (up to 90% for water). These effects change surface water temperature values of ± 2 º C (Kay et al., 2005) considering a constant water emissivity. Radiance values must be corrected according to:

$$L_{\lambda(T_s)} = \frac{L_\lambda - L_{\lambda up}}{t \cdot \varepsilon_\lambda} - \frac{1 - \varepsilon_\lambda}{\varepsilon_\lambda} \cdot L_{\lambda down} \quad (9)$$

Where:

L_λ = uncorrected spectral radiance calculated in Eq. (1).

$L_{\lambda up}$ = upwelling radiance

t = atmospheric transmissivity

ε_λ = water emissivity

$L_{\lambda down}$ = downwelling radiance

Atmospheric parameters ($L_{\lambda up}$, t and $L_{\lambda down}$) were obtained from Atmospheric Correction Parameter Calculator (http://www.atmcorr.gsfc.nasa.gov/) which uses MODTRAN simulator (Barsi et al., 2003).

Calculation of surface temperature (Ts), according to Artis and Carnahan, (1982):

$$T_s = \frac{T_{sat}}{1 + \left(\lambda \cdot \frac{T_{sat}}{\rho}\right) \ln \varepsilon} \quad (10)$$

Where:

$\mathbf{T_{sat}}$ = at-sensor radiative temperature (Eq. 2)

λ = effective wavelenght (11.45 μm)

ε = water emissivity

ρ = constant 14380 m*K

$$\rho = h * \frac{c}{\sigma} \quad (11)$$

Where:

σ = Boltzmann´s constant (1.38 * 10 -23 J/K)

h =Planck´s constant (6.26 * 10 -34 J*s)

c = velocity of light (2.998 * 108 m/s)

2.4. Generation of water surface temperature images

For estimation of water surface temperature Landsat 7 ETM+ thermal band 6 Low Gain was used. We choose this band because its range is greater and is not saturated (Suga et al., 2003, Weng et al., 2004, Chander et al., 2009). Temperature values estimated for each image were extracted by interpolating the location of the sampling sites using gvSIG free software.

2.5. Statistical data analysis

From 35 potential points (7 sampling stations and 5 images), only 27 could be included in the analysis for different reasons (lacking of field data, cloud pixel in the images or land-water mixed pixels). At first instance, all points were analyzed together (observed and estimated water surface temperature). Simple regression analysis was made to evaluate the correlation of estimated water surface temperature obtained by AWVM with *in situ* data. In order to enhance the results obtained by the AWVM, the same analysis was performed using the classic method RTM. In addition, for the determination of significant differences between estimated and observed temperature values, Chi Square statistic test was applied.

3. Results and discussion

Values of estimated and observed water surface temperatures obtained by the two compared methods were correlated applying a simple regression model. Correlation coefficients were significant (R^2: 0.9426 for AWVM method and R^2: 0.9584 for RTM method) while their standard errors were acceptable in both cases. Both models showed very good adjustment, although the RTM fits slightly better (Table 2, Figs. 2A and 2B). Chi Square analysis performed to test these results showed that estimations were accurate (Table 3).

Analysis of data in a time sequence allowed a more detailed e of the accuracy of AWVM. *In situ* and RTM data were included to compare results (Fig. 3). The temperature values estimated by AWVM were higher than those for the RTM (Figs. 3A, 3B, 3C and 3E), although following the same trend that matches the behavior of *in situ* values. Both methods have overestimated observed values, except for data of July 2006, when field measurements were underestimated. This situation occurs because in winter there is a greater temperature difference between the colder air layer just above the water and the most superficial water layer. As a consequence both methods lost accuracy; however the trend curves continue being coherent. In August 2002, AWVM overestimated *in situ* data in two of the three sampling stations. At sites D, G, C and PM2, the differences were minor while in the remaining sites (PAA, PC and PM1) differences were higher (up to 3 º C).

Differences in surface water temperature estimated in stations close to (PM1 and PM2) and far from (G) the cooling channel are in agreement with the conclusions of Mariñelarena et al. (annual reports). In all cases the estimated temperatures at station PM1 were higher than those at PM2 and these were higher than those at station G, following a dissipation line from the cooling channel outlet to the lake (Fig. 3).

We built the water surface temperature maps based on AWVM (Fig. 4) considering the obtained results and the fact that AVWM has important advantages over RTM (simple atmospheric data for correction and possibility of application to different thermal sensors).

4. Conclusions

AWVM and RTM methods adequately estimated water surface temperature in Embalse del Río Tercero. Nevertheless, AWVM could estimate rather small differences in temperature between sites consistently with the results obtained in field measurements. So we conclude that AWVM is the most suitable method for monitoring the thermal plume in this reservoir using satellite imagery. Besides, as mentioned above, this method has the advantage that it only uses values of

atmospheric water vapor and it can be applied to different thermal sensors using the same equation and coefficients.

This adaptation of the generalized single-channel method developed by Jiménez-Muñoz and Sobrino (2003) provides a simpler tool for the calculation of water surface temperature in this waterbody and expands the possibilities of application in other places with Landsat images or other existing sensors.

5. References

- Ahn, Y., Shanmugam P., Lee J., Kang Y. Application of satellite infrared data for mapping of thermal plume contamination in coastal ecosystem of Korea. Marine Environmental Research. 61, 186–201, 2006.
- Alcântara, E., Barbosa C., Stech, J., Novo, E., Shimabukuro Y. Improving the spectral unmixing algorithm to map water turbidity distributions. Environmental Modelling and Software. 24, 1051−1061, 2009.
- Alcântara, E., Stech J., Lorenzzetti, J., Bonnet, M. P., Casamitjana, X., Assireu A. T. , Novo, E. Remote sensing of water surface temperature and heat flux over a tropical hydroelectric reservoir. Remote Sensing of Environment. 114 (11), 2651-2665, 2010.
- Artis, D. A., Carnahan, W. H. Survey of emissivity variability in thermography of urban areas. Remote Sensing of Environment. 12, 313-329. 1982.
- Barsi, J. A., Barker J. L., Schott J. R. An Atmospheric Correction Parameter Calculator for a Single Thermal Band Earth-Sensing Instrument. IGARSS03, 21-25 July 2003, Centre de Congres Pierre Baudis, Toulouse, France. 2003.
- Becker, F., Li, Z. L. Surface Temperature and emissivity at various scales: definition, measurement and related problems. Remote Sensing Reviews.12, 225-253. 1995
- Becker, M. W., Daw, A. Influence of lake morphology and clarity on water surface temperature as measured by EOS ASTER. Remote Sensing of Environment. 99, 288-294.2005.
- Casamitjana, X., Serra T., Baserba, C., Pérez-Losada, J. Effects of the water withdrawal on the stratification patterns of a reservoir. Hydrobiologia, 504, 21-28. 2003.
- Chander, G., Markham, B. L., Helder, D. L. Summary of current radiometric calibration coefficients for Landsat MSS, TM, ETM+, and EO-1 ALI sensors. Remote Sensing of Environment, 113, 893–903. 2009.
- Cherkauer K. A., Burges S. J., Handcock, R.N., Kay, J.E., Kampf, S.K., Gillespie, A. R. Assessing Satellite-Based and Aircraft-Based Thermal Infrared Remote Sensing for Monitoring Pacific Northwest River Temperature. Journal of the American Water Resources Association (JAWRA). 41(5), 1149-1159. 2005.
- Chuvieco, E. Teledetección Ambiental (Environmental Remote Sesning). 1st Ed. Ariel S.A., Barcelona, Spain. 586 pp. 2002. (in Spanish).
- Cooper, D. I., Asrar G. Evaluating atmospheric correction models for retrieving surface temperatures from the AVHRR over a tallgrass prairie. Remote Sensing of Environment, 27, 93–102. 1989.
- Dash P., Göttsche, F. M., Olesen F. S., Fischer H. Land surface temperature and emissivity estimation from passive sensor data: theory and practice-current trends. International Journal of Remote Sensing. 23, 2563-2594. 2002.

- Donlon, C. J., Minnett P., Gentemann, C. Towards improved validation of satellite sea surface skin temperature measurements for climate research. *Journal of Climate*, 15, 353-369. 2002.
- Gibbons, D. E., Wukelic, G. E. Application of Landsat thematic mapper data for coastal thermal plume analysis at Diablo Canyon. Photogrammetric Engineering and Remote Sensing, 55, 903–909. 1989.
- Gillespie, A., Rokugawa, S., Matsunaga T., Cothern J. S., Hook S., Kahle, A. B. A temperature and emissivity separation algorithm for advanced spaceborne thermal emission and reflection radiometer (ASTER) images. IEEE Transactions on Geoscience and Remote Sensing, 36, 1113–1126. 1998.
- Goïta, K., Royer A. Surface temperature and emissivity separability over land surface from combined TIR and SWIR AVHRR data, IEEE Transactions on Geoscience and Remote Sensing, 35 (3). 1997.
- Irish, R. R. Landsat 7 Science Data Users Handbook. National Aeronautics and Space Administration (NASA). Report Nº 430-15-01-003-0. 2006.
- Jiménez- Muñoz J. C. , Sobrino, J. A. A generalized single-channel method for retrieving land surface temperature from remote sensing data. Journal of Geophysical Research, 108 (D22), doi: 10.1029/2003JD003480). 2003.
- Kay, J. E., Kampf S. K., Handcock, R. N., Cherkauer, K. A., Gillespie, A. R., Burges S. J. Accuracy of lake and stream temperatures estimated from thermal infrared images. Journal of the American Water Resources Association, 41, 1161-1175. 2005.
- Kimmel, B. L., Lind, O. T., Paulson L. J. Reservoir primary production. In K. W. Thorton, Kimmel, B. L., Payne F. E. (Eds.), Reservoir limnology. Ecological Perspectives. John Wiley and Sons. New York. 1990.
- Kishino, M., Matsunaga, T., Abrams, M., Kato, M. Water quality and temperature mapping using ASTER. International Geoscience and Remote Sensing Symposium (IGARSS) 2000, Honolulu, Hawaii. 2000.
- Kumar, A., Minnett, P. J., Podestá, G., Evans, R. H. Characteristics of the Atmospheric Correction Algorithms Used in Retrieval of Sea Surface Temperatures From Infrared Satellite Measurements: Global and Regional Aspects. Journal of the Atmospheric Sciences, 60, 575-585. 2003.
- Mariazzi, A. A., Romero, M. C., Villalobos, E. R. Di Siervi, M. A., Mariñelarena, A. Estudio bacteriológico en el Embalse del Río III (Provincia de Córdoba, Argentina). Factores ecológicos, predicciones sobre efectos térmicos. Limnobios, 2, 89-110. 1981. (In Spanish).
- Mariazzi, A. A., Romero, M. C., Conzonno, V. H., Mariñelarena, A. Results of a limnological study in a reservoir previous to the functioning of a nuclear power plant (Embalse del Rio III). Revista de la Asociación de Ciencias Naturales del Litoral, 20 (1 and 2), 57-68. 1989.
- Mariazzi, A. A., Donadelli, J. L., Arenas, P., Di Siervi, M. A., Bonetto, C. Impact of a nuclear power plant on water quality of Embalse del Río Tercero Reservoir, (Córdoba, Argentina). Hydrobiologia, 246, 129-140. 1992
- Mariñelarena, A. J., Casco, M. A., Claps, M. C. , Di Siervi, M. A. , Donadelli J. L., Hechem, M. A., Mac Donagh, M. E., Ardohain, D. M. Estudio Limnológico del Embalse del Río Tercero, (Córdoba). Annual reports to Central Nuclear Embalse. 1996 – present. (In Spanish).
- Mustard, J. F., M. A. Carney, Sen, A. The use of satellite data to quantify thermal effluent impacts. Estuarine, Coastal and Shelf Science, 49, 509-524. 1999.
- Novo, E. L, Barbosa, C. C. F., Freitas R. M., Shimabukuro Y. E., Melack J. M., Pereira-Filho, W. Seasonal changes in chlorophyll distribution in Amazon floodplain lakes derived from MODIS images. Limnology, 7, 153−161. 2006.

- Schneider, K , Mauser, W. Processing and Accuracy of Landsat Thematic Mapper Data for Lake Surface Temperature Measurement. International Journal of Remote Sensing, 17, 2027–2041. 1996.
- Snyder, W. C., Wan Z., Zhang Y., Feng Y. Z. Classification-based emissivity for land surface temperature measurement from space. International Journal of Remote Sensing, 19(14), 2753-2774. 1998.
- Sobrino, J. A., Raissouni., N. Toward remote sensing methods for land cover dynamic monitoring, Application to Morocco, International Journal of Remote Sensing,20, 353– 366. 2000.
- Suga, Y., Ogawa, H., Ohno K., K. Yamada. Detection of surface temperature from Landsat 7 ETM+. Advances in Space Research, 32(11), 2235-2240. 2003.
- Wang, L. T., McKenna, T. E., DeLiberty, T. L. Locating Ground water discharge areas in Rehoboth and Indian river bays and Indian river, Delaware using Landsat 7 imagery. Report of Investigations Nº 74. University of Delaware and Delaware Geological Survey: 17. 2008.
- Weng, Q., Lu, D., J. Schubring. Estimation of Land Surface Temperature vegetation abundance relationship for urban heat island studies. Remote Sensing of Environment, 89, 467-483. 2004.
- Wukelic, G. E., Gibbons D. E., I. M. Martucci, Foote, H.P. Radiometric calibration of Landsat Thematic Mapper Thermal Band. Remote Sensing of Environment, 28, 339-347. 1989.
- Yokoyama, R., Tanba S. , Souma T. Sea surface effects on the sea surface temperature estimation by remote sensing. International Journal of Remote Sensing, 16, 227–238. 1995.
- Zoran M. A., Nicola D. N., Talianu, C. L, Ciobanu, M., Ciuciu J. G. Analyses of thermal plume of Cernavoda nuclear power plant by satellite remote sensing data. Proceedings of the Remote Sensing for Environmental Monitoring, GIS Applications, and Geology V. Manfred Ehlers and Ulrich Michel (Eds.). 2005.

Figure Captions:

Figure 1. Location of the sampling stations in the Río Tercero Reservoir. References: D: Dique, G: Garganta, C: Confluencia, PM1: Pluma M1, PM2: Pluma M2, PC: Pluma Canal, PAA: Pluma Aguas Arriba.

Figure 2. Plot of estimated water surface temperature versus measured water surface temperature. A. Atmospheric Water Vapour Method (AWVM). B. Radiative Transfer Method (RTM).

Figure 3. Comparison of measured and estimated water surface temperature with RTM and AWVM over sampling stations: A. March 19th, 2000, B. August 13rd, 2001, C. August 16th, 2002, D. July 10th, 2006 and E. November 15th, 2006.

Figure 4. Water surface temperature maps (ºC). A. March 19th, 2000, B. August 13rd, 2001, C. August 16th, 2002, D. July 10th, 2006 and E. November 15th, 2006.

Table Captions:

Table 1. Gains and Biases of Landsat 7 ETM+ thermal bands.

Table 2. Regression statistics of comparison between measured and estimated water surface temperature from both methods.

Table 3. Chi Square test for comparison between measured and estimated water surface temperature from both methods. Critical value: $p<0.05$ 38.885.

Table

Click here to download high resolution image

Satellite/Sensor	Band	Gain ($W/m^2*sr*\mu m$)/DN	Bias $W/m^2*sr*\mu m$	Source
Landsat 7 ETM+	6 Low gain[a]	0.067087	−0.07	Chander *et al.*, 2009
	6 High gain	0.037205	3.16	

Table

Click here to download high resolution image

Methods	Multiple R^2	Adjusted R^2	Standard error of estimate	F	P(x)	n
AWVM	0.949855	0.940262	1.224921013	410.2304	0	27
RTM	0.958384	0.956719	1.042623618	575.7314	0	27

Table

Click here to download high resolution image

Methods	Chi Square	Degree of freedom	P(x)
AWVM	2.869466	26	<1
RTM	1.883663	26	<1

Figure

Click here to download high resolution image

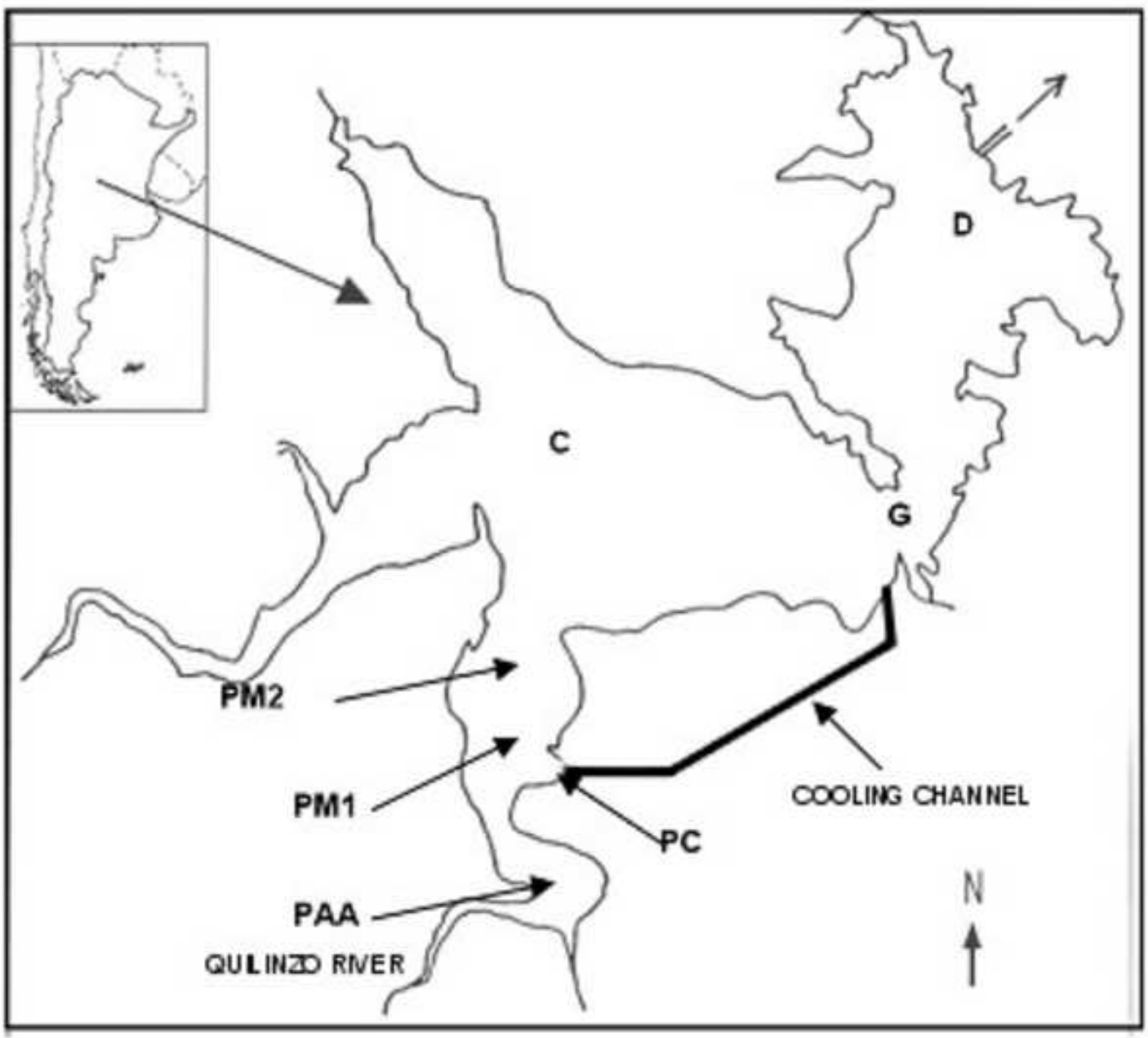

Figure

Click here to download high resolution image

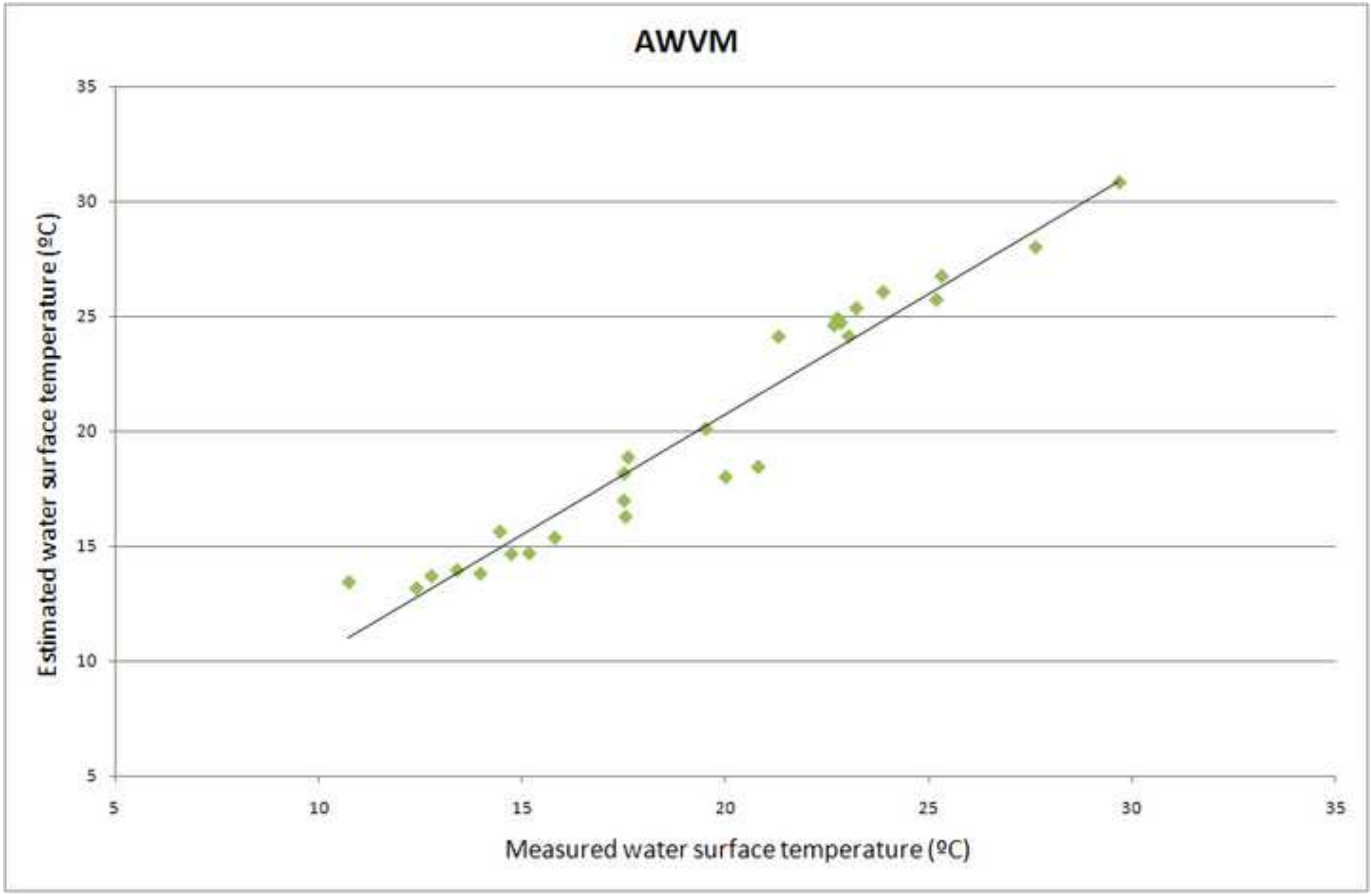

Figure

Click here to download high resolution image

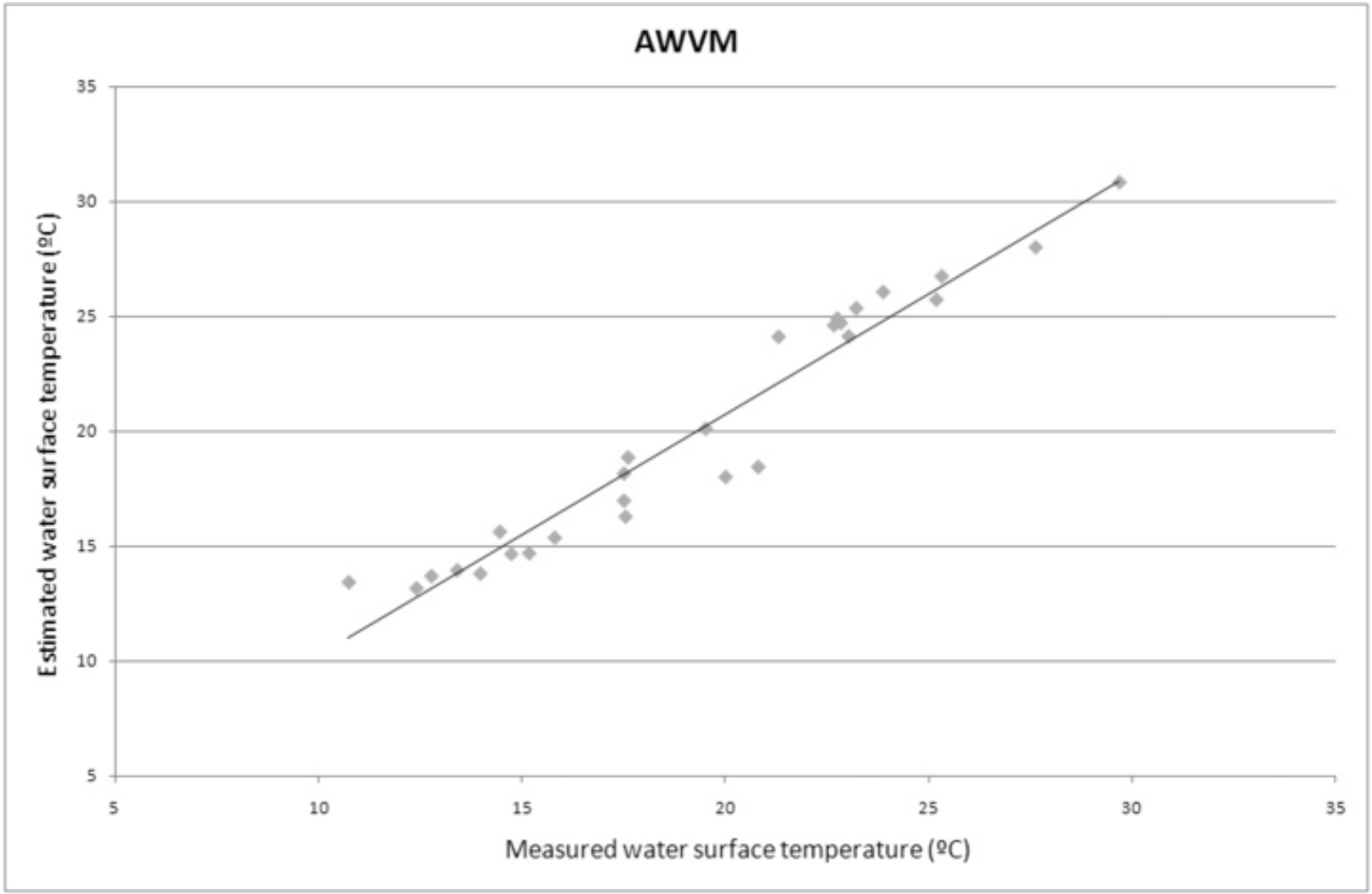

Figure

Click here to download high resolution image

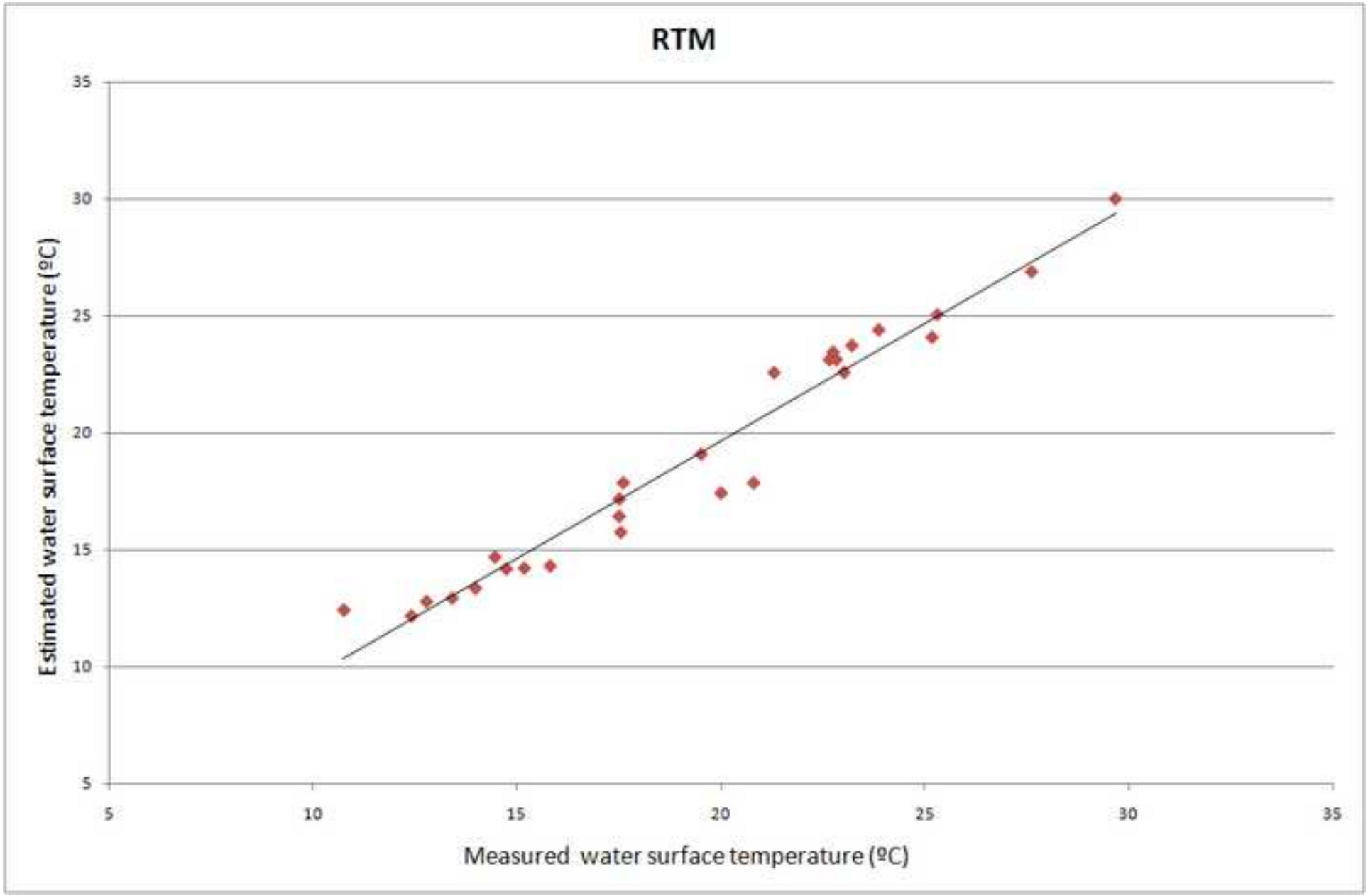

Figure

Click here to download high resolution image

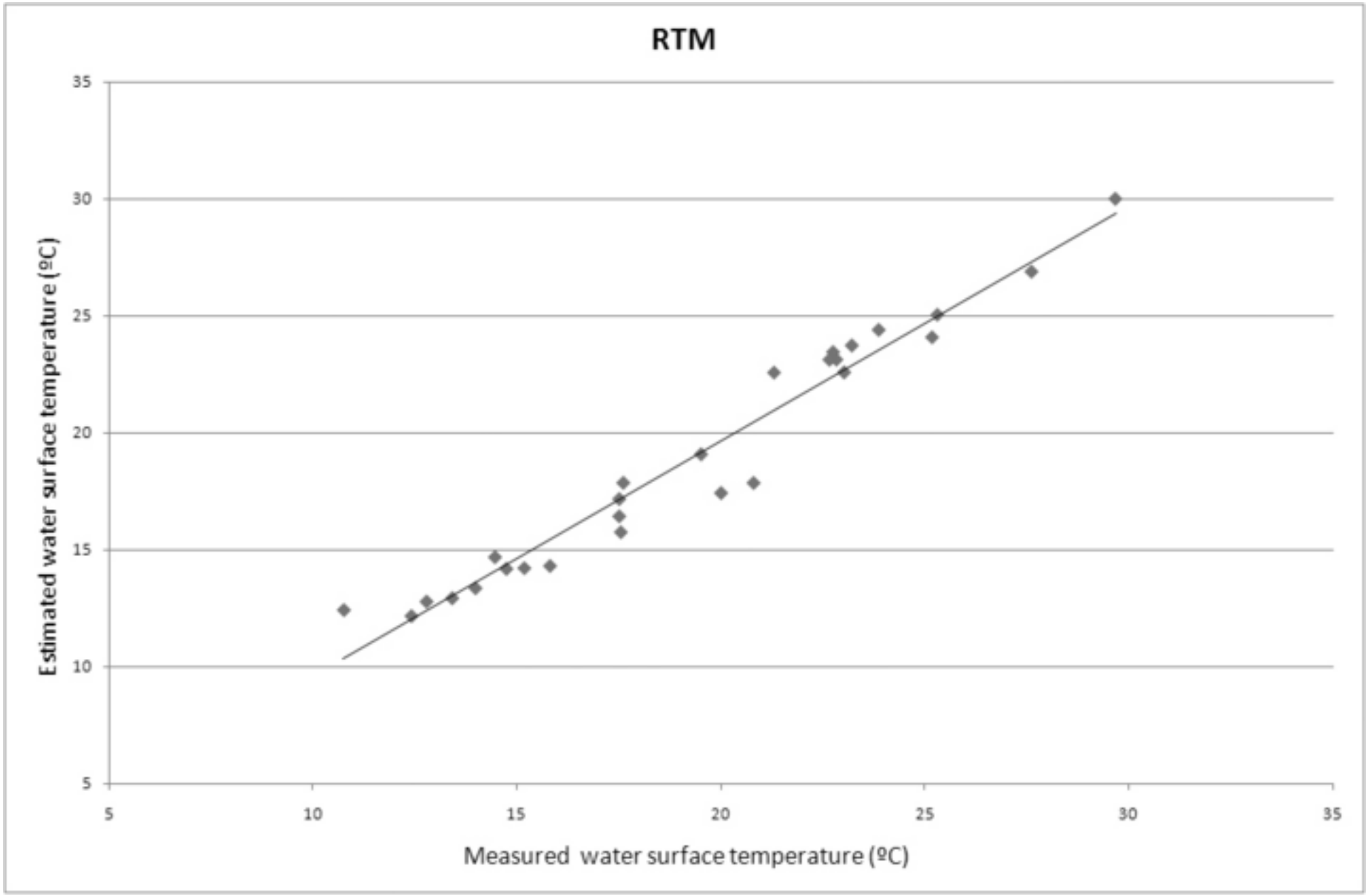

Figure

Click here to download high resolution image

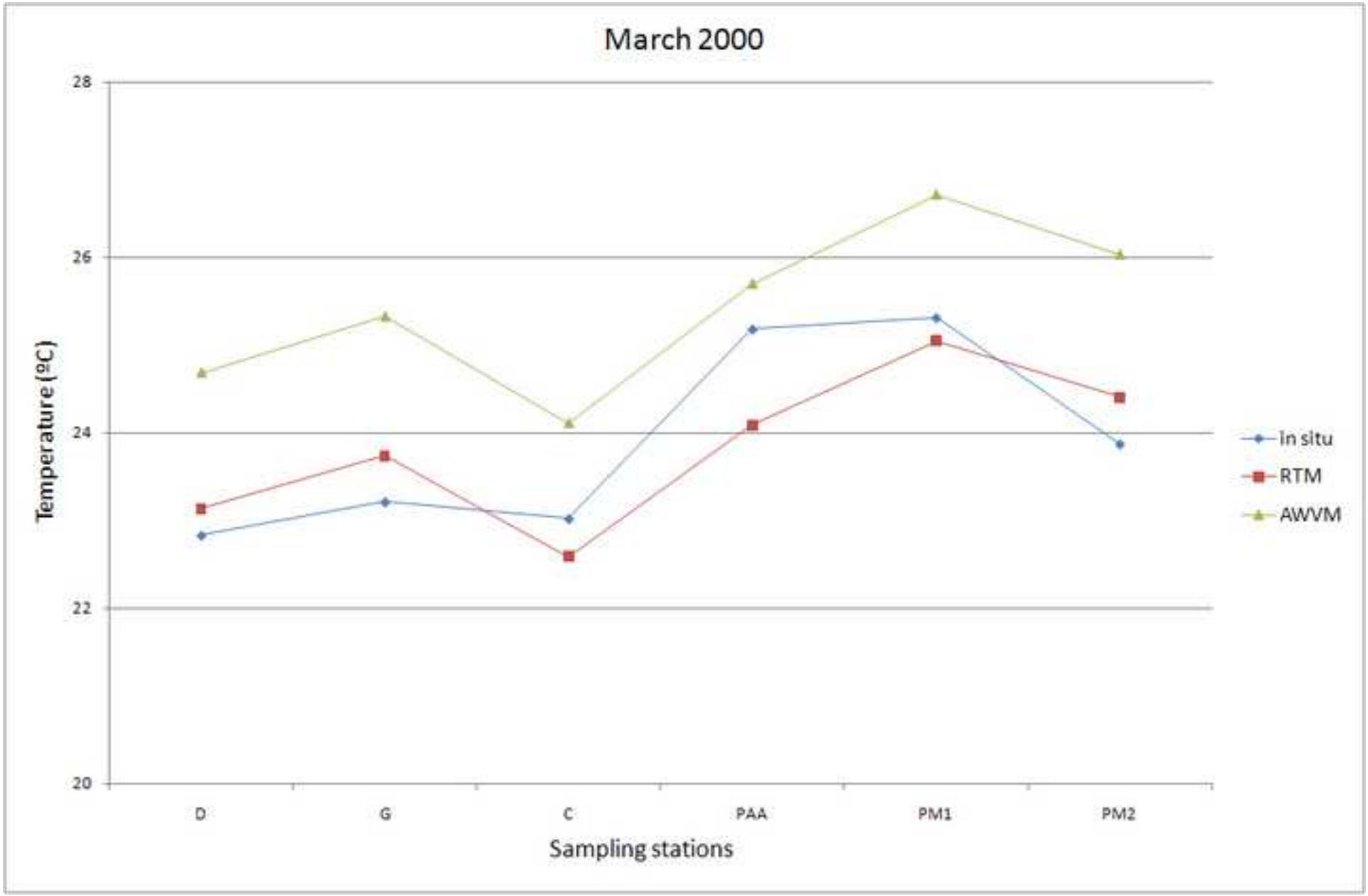

Figure

Click here to download high resolution image

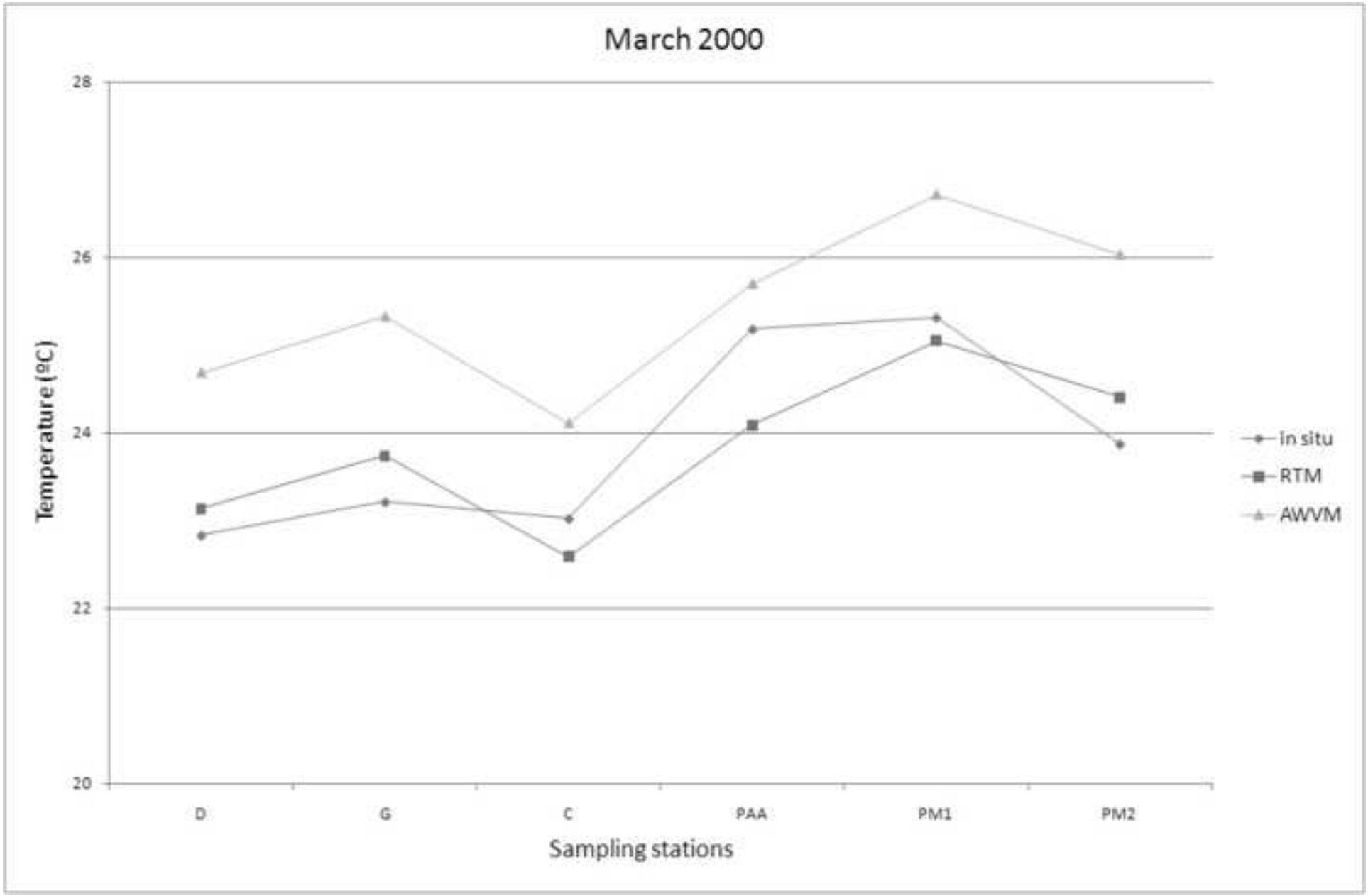

Figure

Click here to download high resolution image

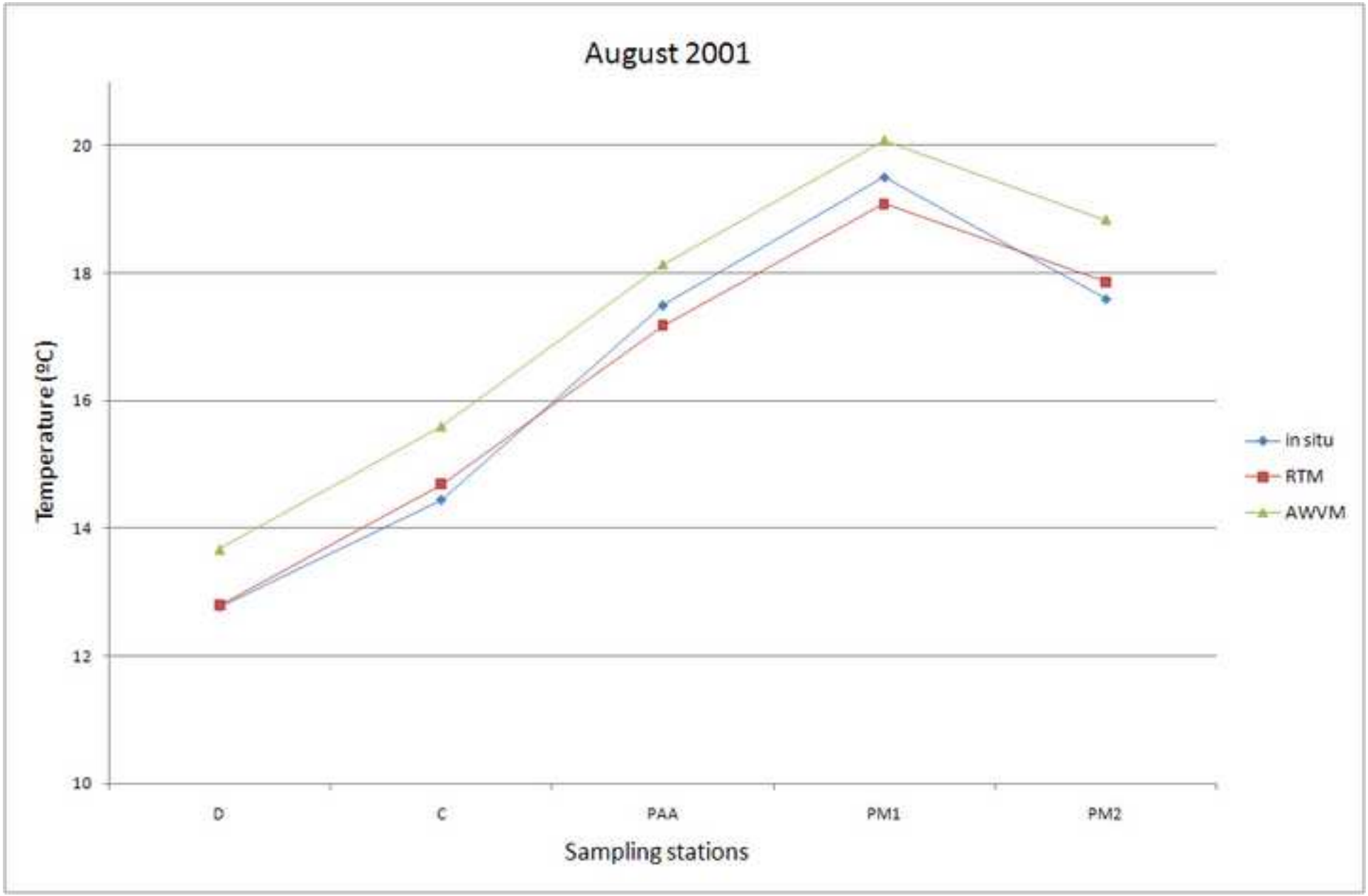

Figure

Click here to download high resolution image

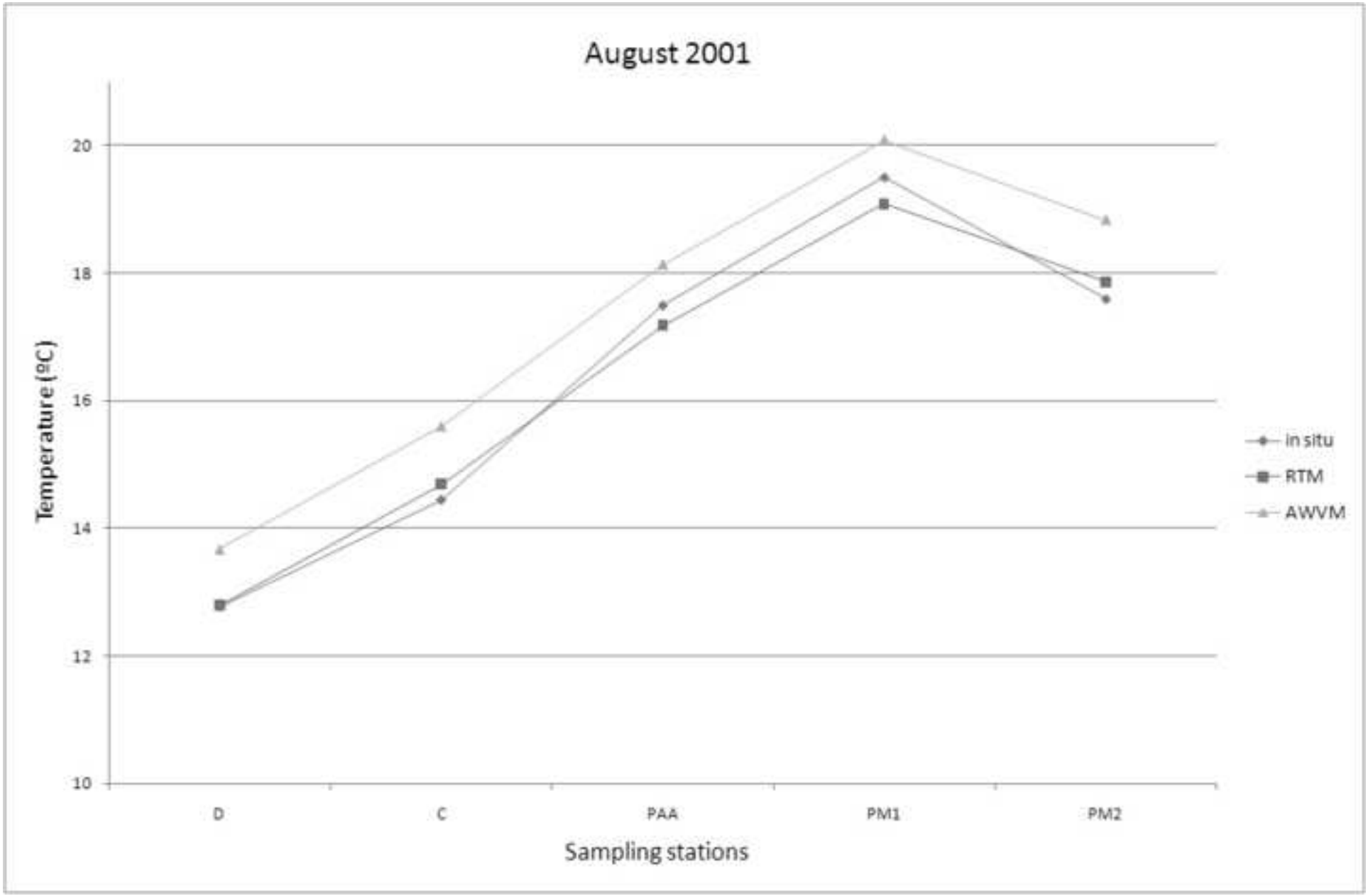

Figure
Click here to download high resolution image

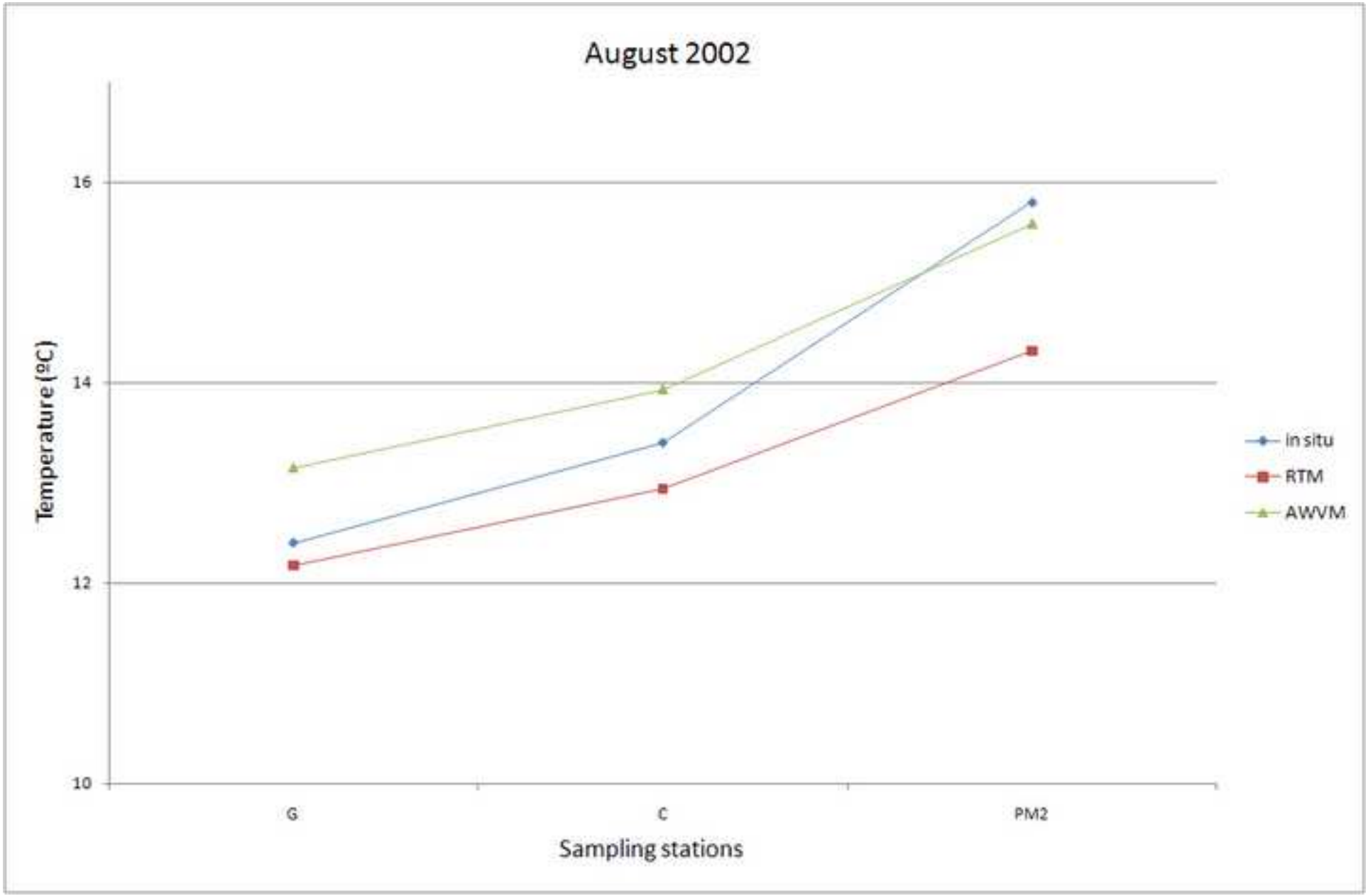

Figure

Click here to download high resolution image

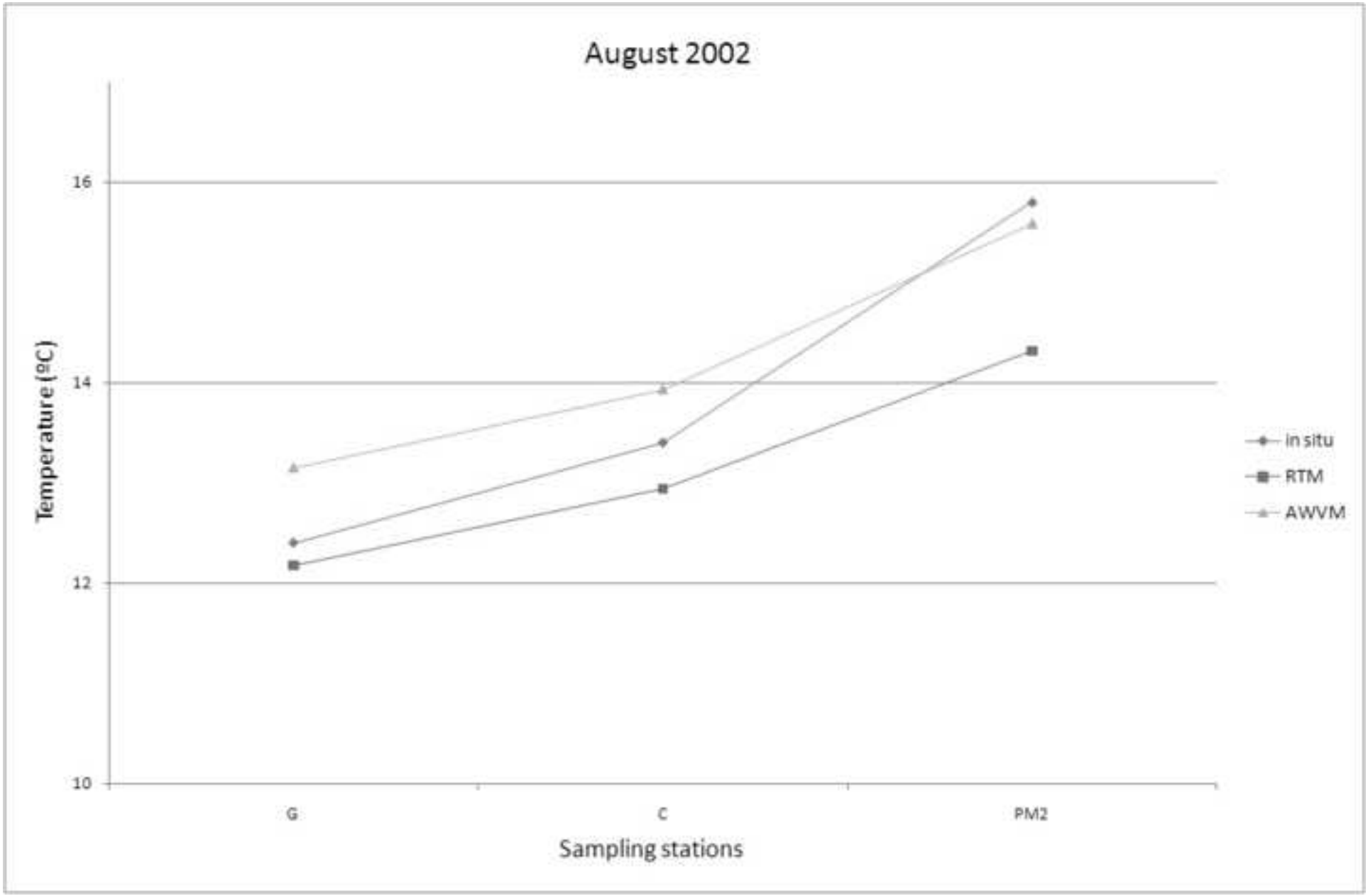

Figure

Click here to download high resolution image

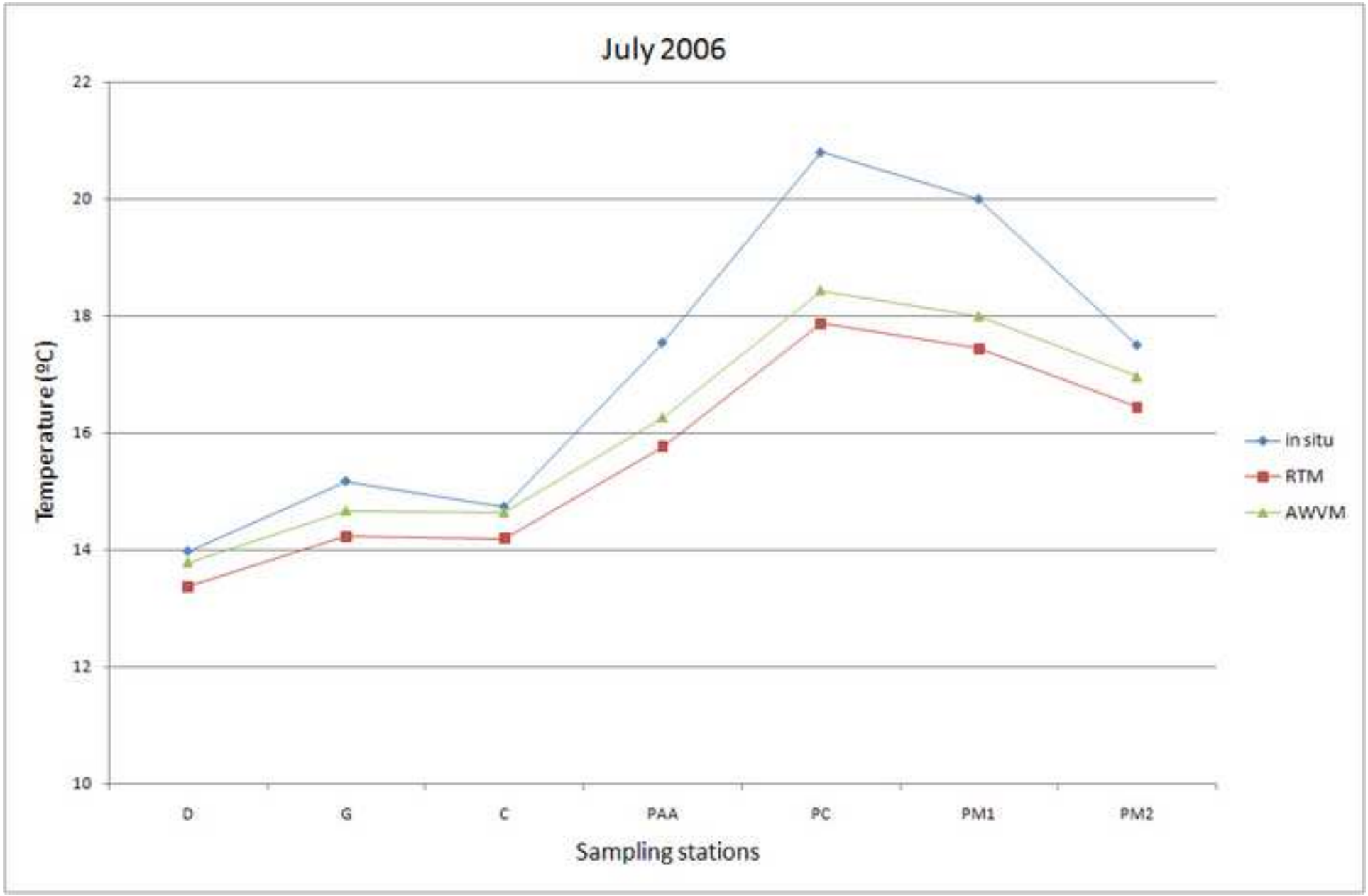

Figure

Click here to download high resolution image

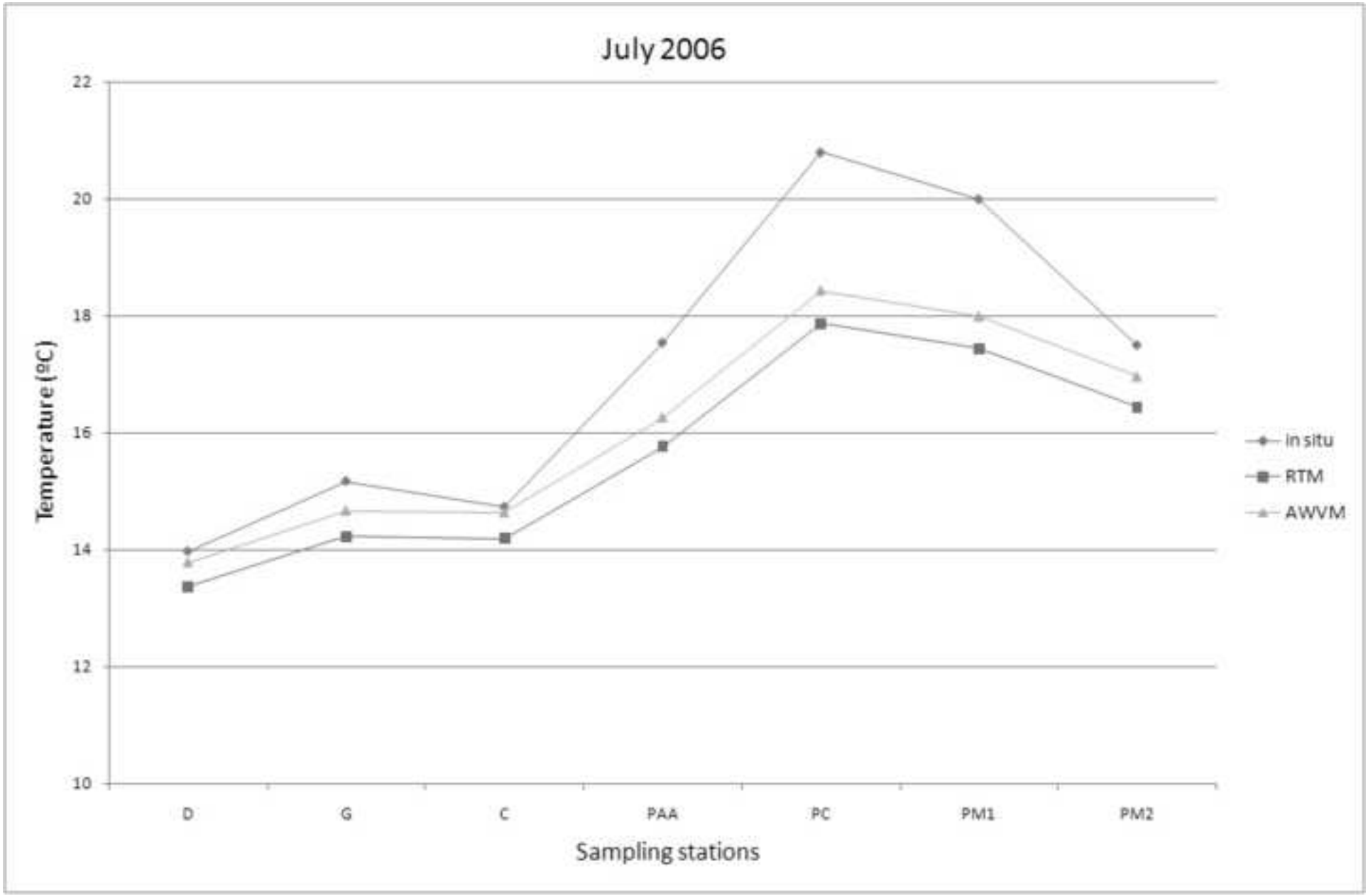

Figure

Click here to download high resolution image

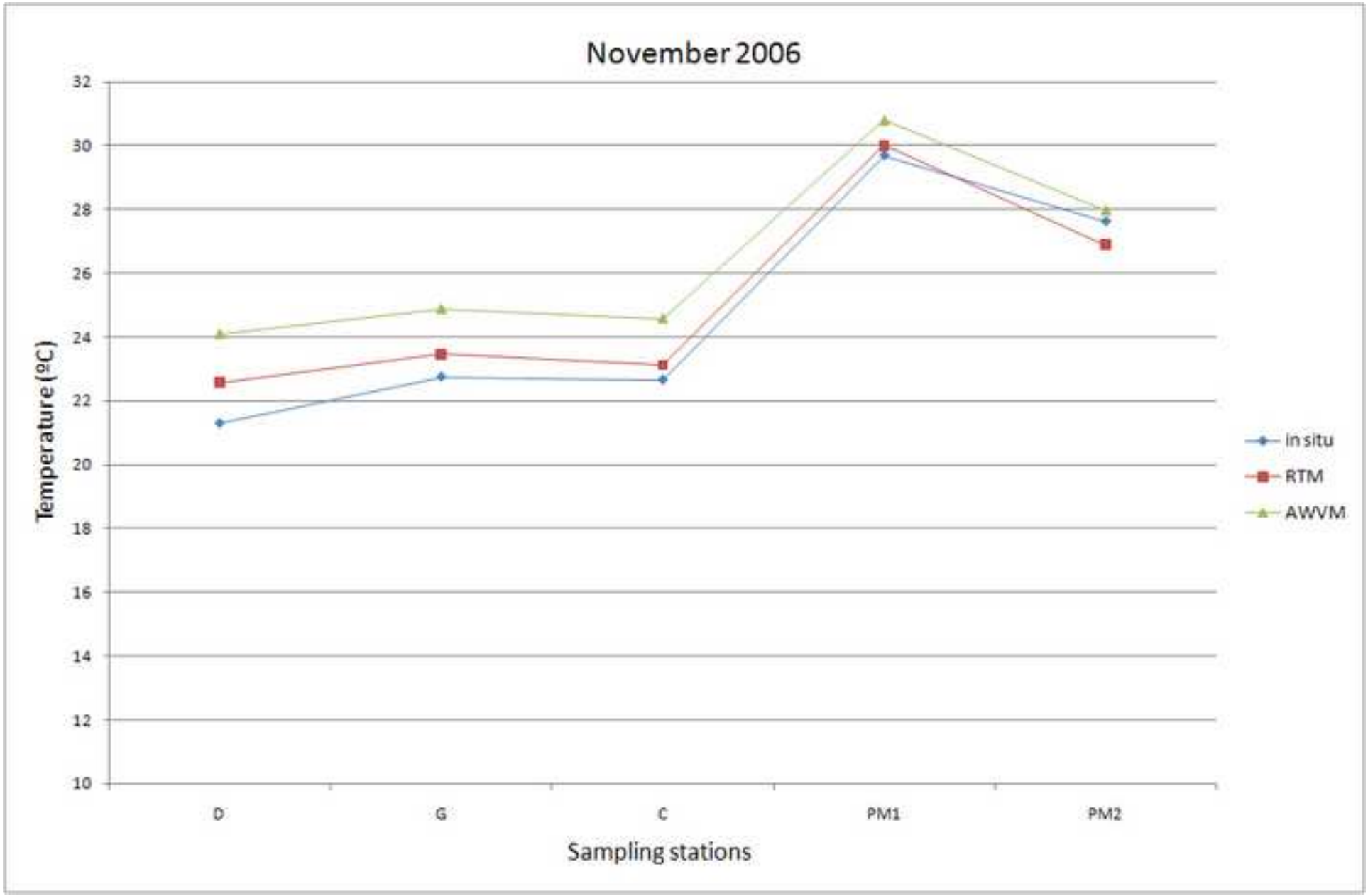

Figure

Click here to download high resolution image

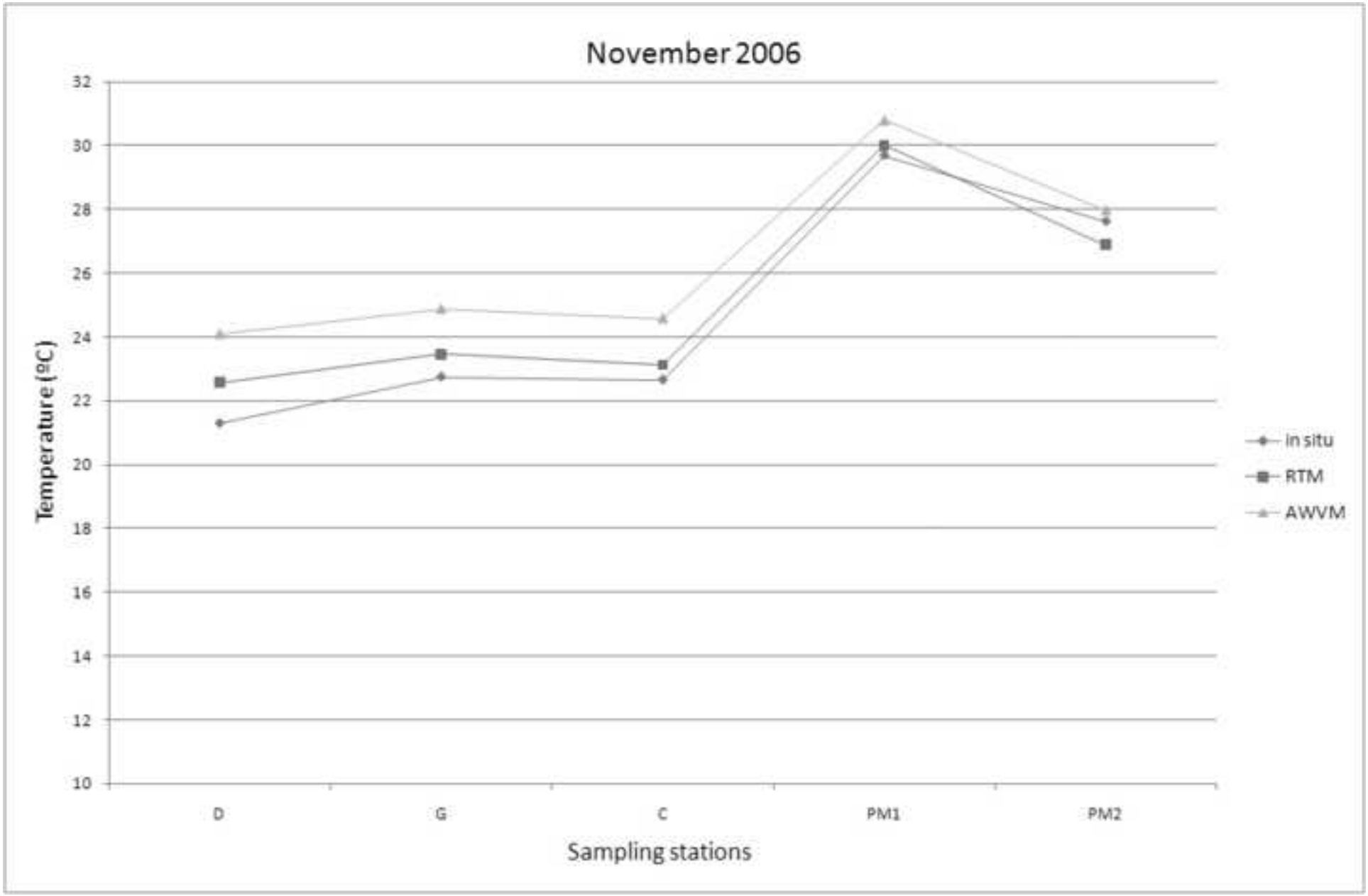

Figure

Click here to download high resolution image

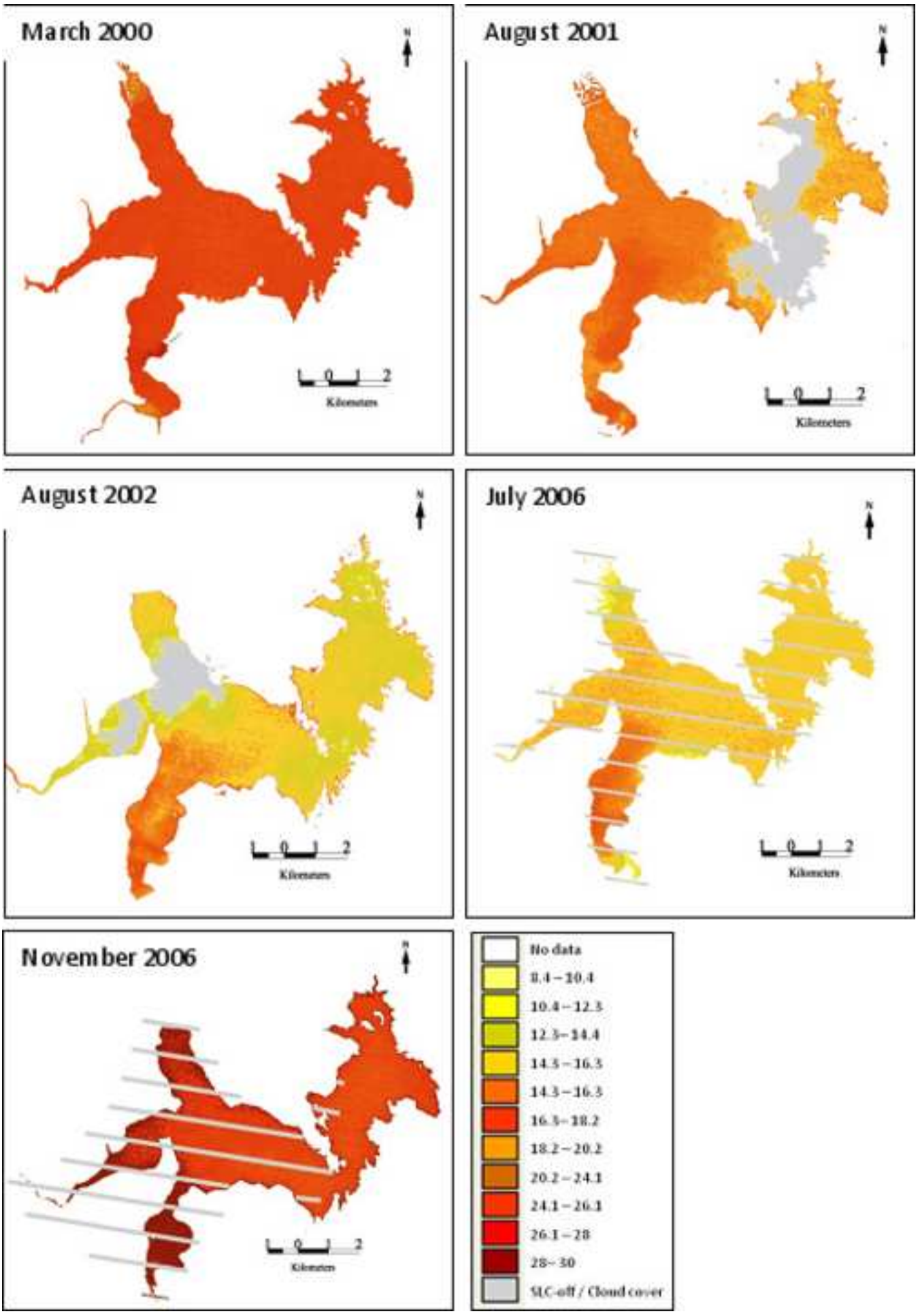

Figure

Click here to download high resolution image

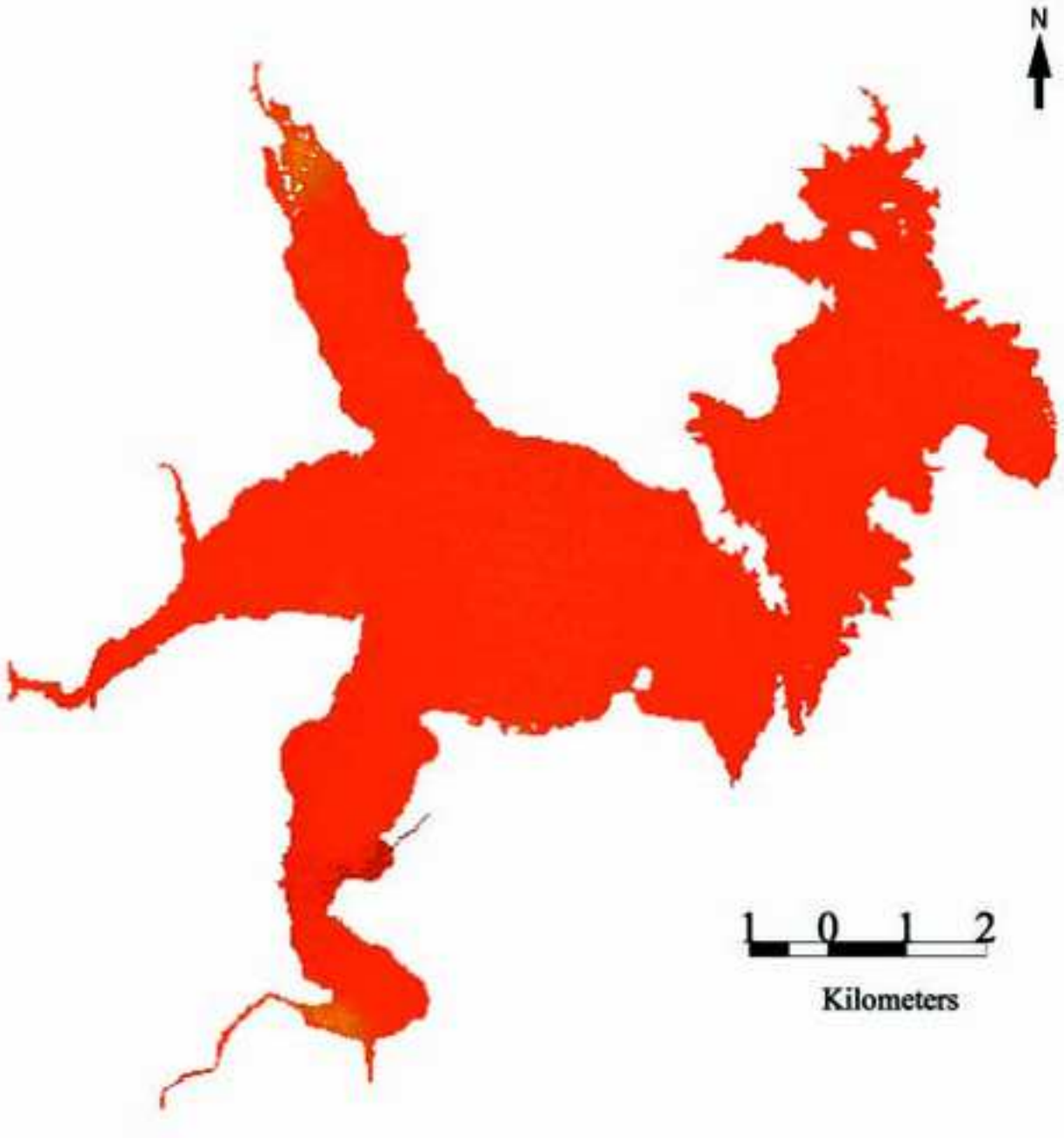

Figure

Click here to download high resolution image

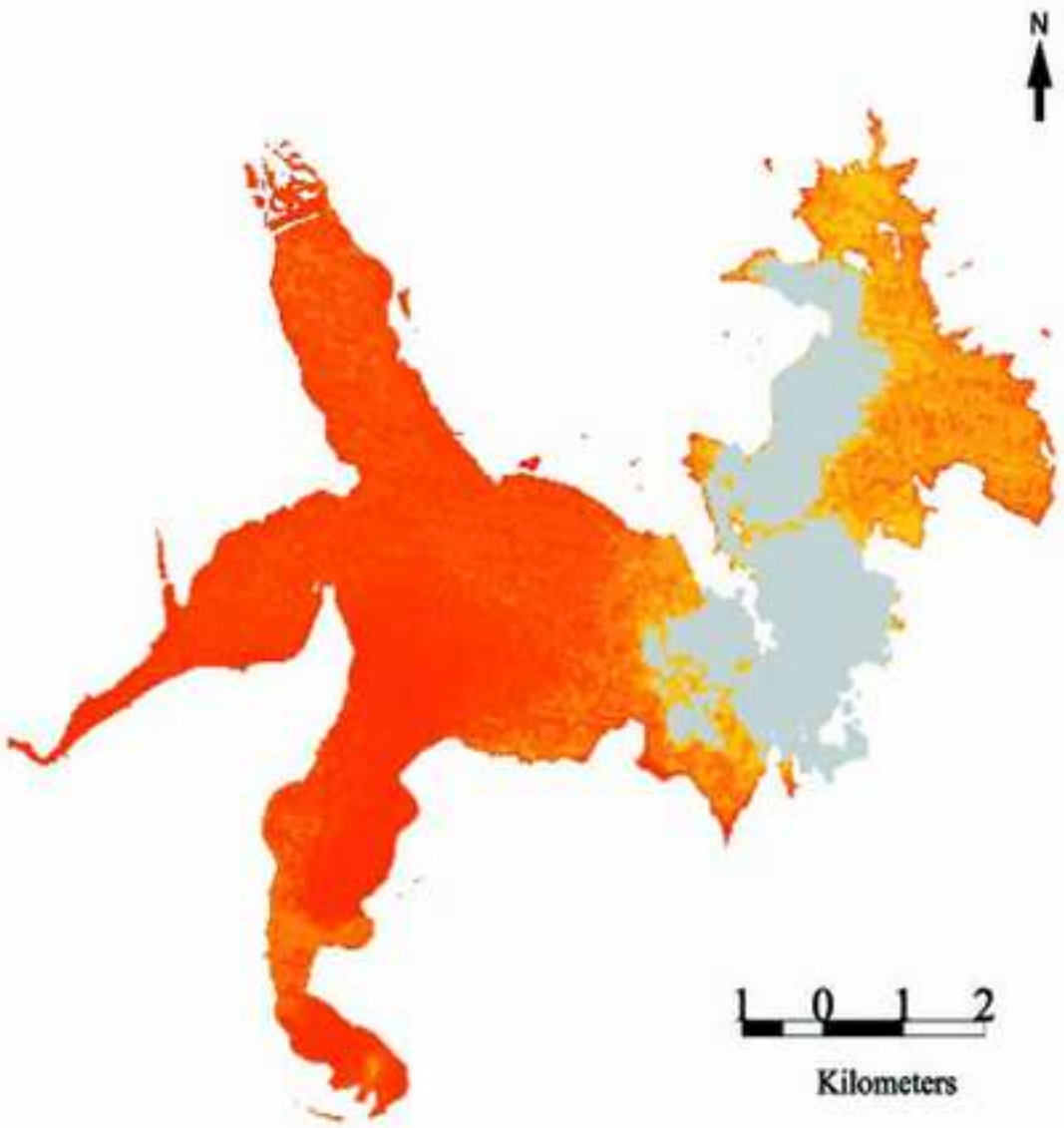

Figure

Click here to download high resolution image

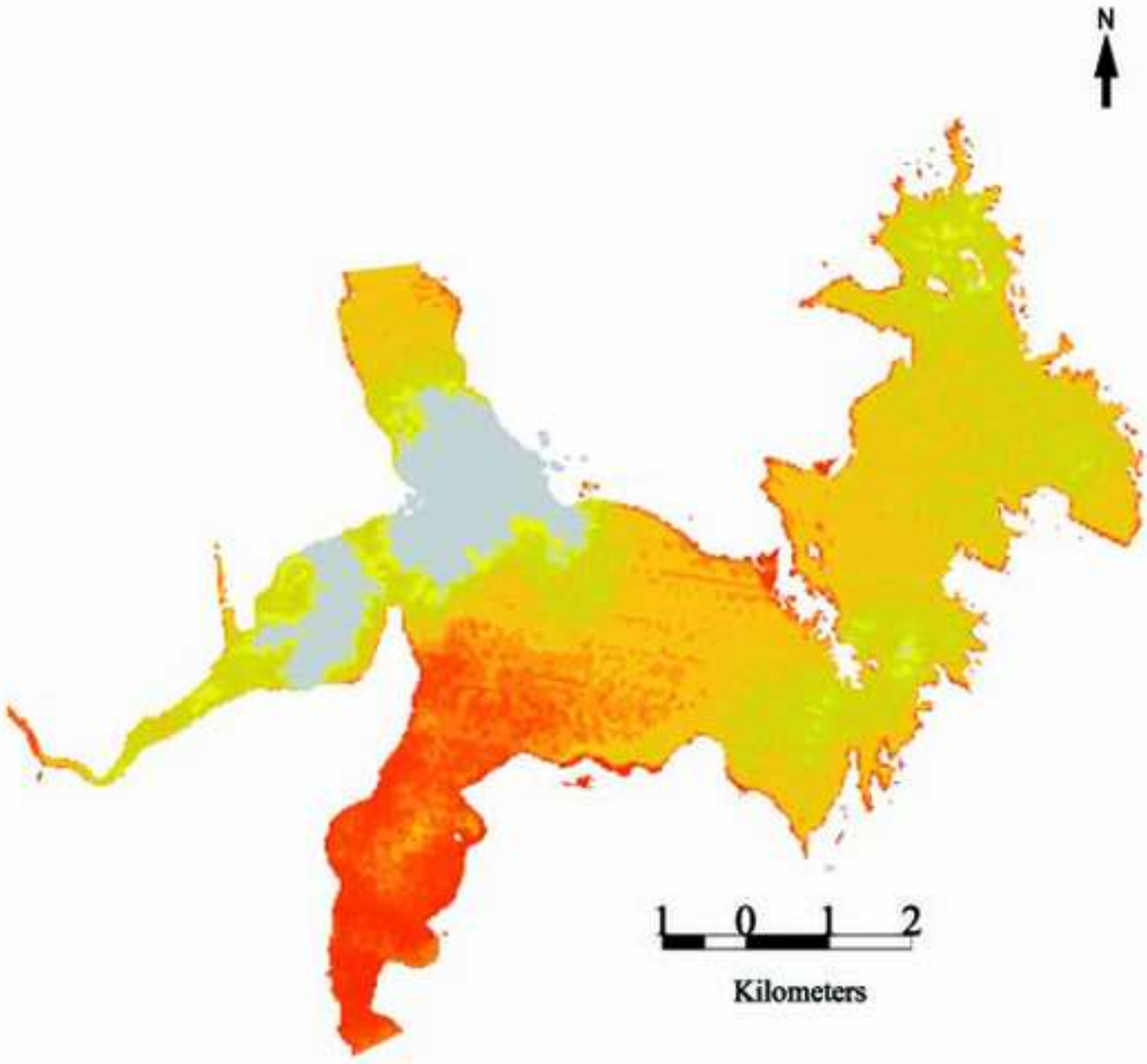

Figure
Click here to download high resolution image

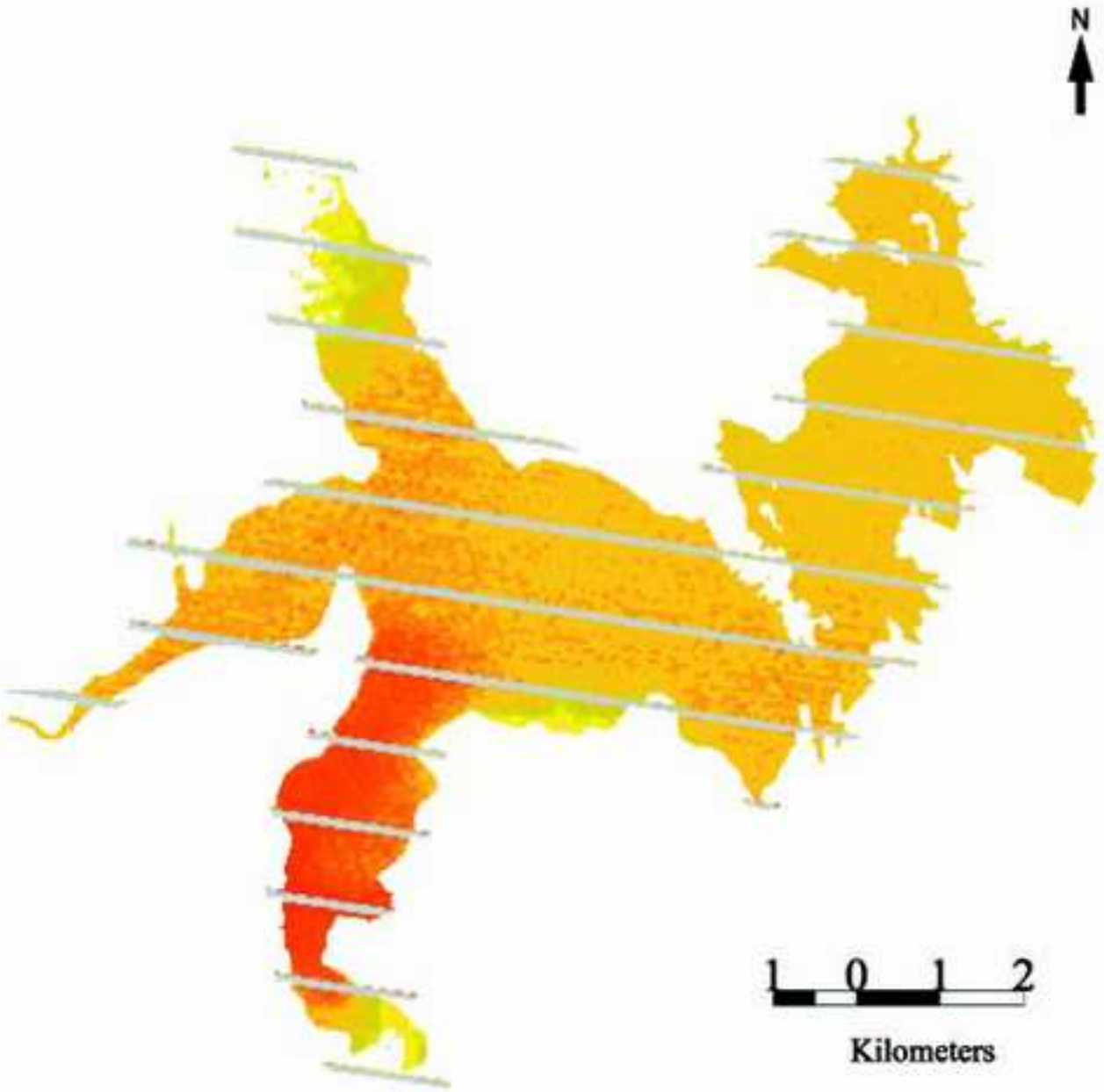

Figure

Click here to download high resolution image

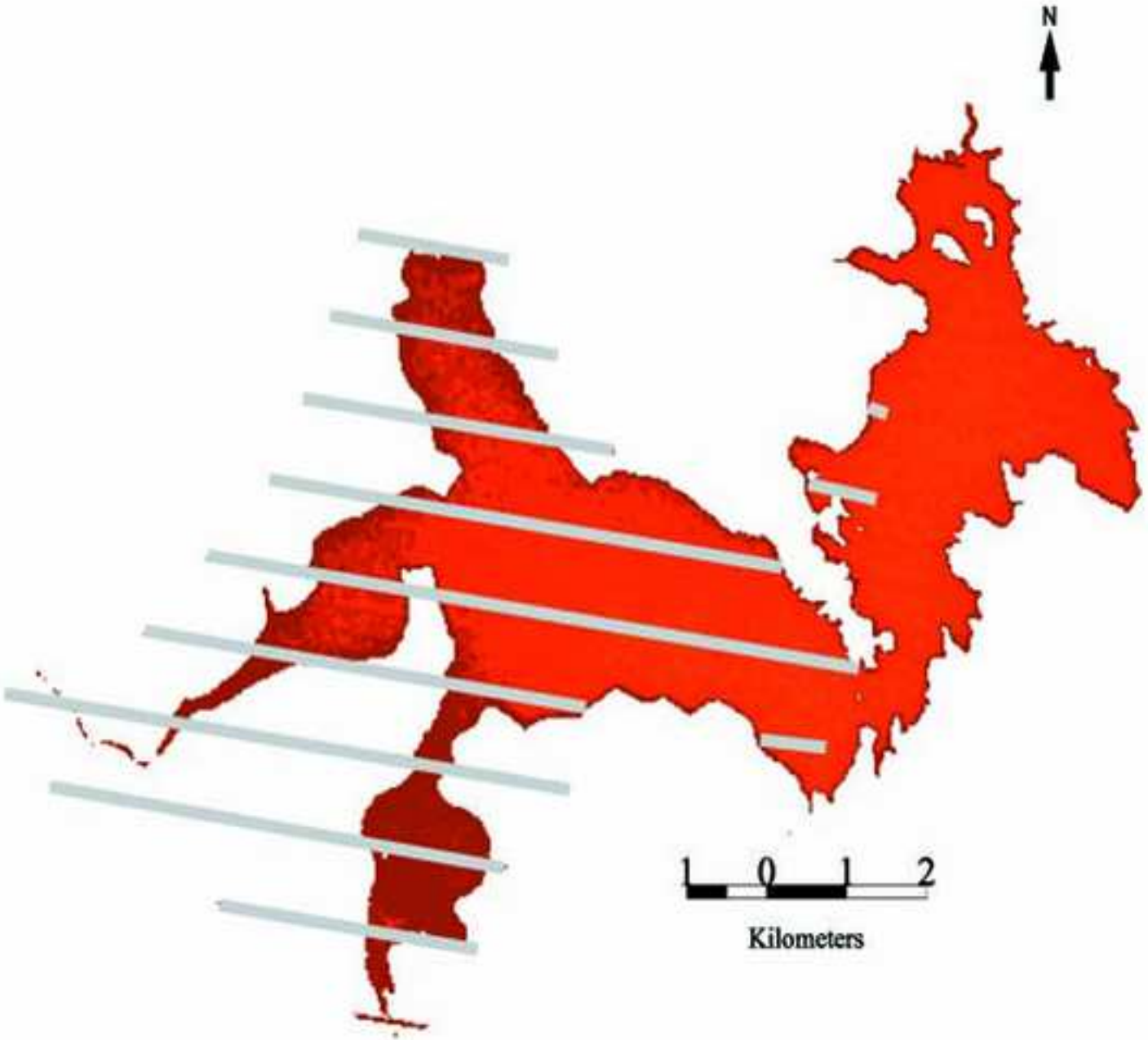

Figure

Click here to download high resolution image